Title:

Dual-specific autophosphorylation of kinase IKK2 enables phosphorylation of substrate IκBα through a phosphoenzyme intermediate

Prateeka Borar[1], Tapan Biswas[2,#], Ankur Chaudhuri[3,#], Tom Huxford[4], Saikat Chakrabarti[3] Gourisankar Ghosh[2] & Smarajit Polley[1,*]

[1]Department of Biological Sciences, Bose Institute, Kolkata, India; [2]Department of Chemistry and Biochemistry, University of California San Diego, La Jolla, USA; [3]Structural Biology and Bioinformatics Division, CSIR-Indian Institute of Chemical Biology, Kolkata, India; [4]Department of Chemistry and Biochemistry, San Diego State University, San Diego, USA.

[#] These two authors have contributed equally to this work.

*Correspondence to be addressed to: spolley@jcbose.ac.in, smarajit.polley@gmail.com

Abstract:

Rapid and high-fidelity phosphorylation of two serines (S32 and S36) of IκBα by a prototype Ser/Thr kinase IKK2 is critical for fruitful canonical NF-κB activation. Here, we report that IKK2 is a dual specificity kinase that autophosphorylates itself at tyrosine residues in addition to its activation loop serines. Mutation of one such tyrosine, Y169, located in proximity to the active site, to phenylalanine, renders IKK2 inactive for phosphorylation of S32 of IκBα. Surprisingly, auto-phosphorylated IKK2 relayed phosphate group(s) to IκBα without ATP when ADP is present. We also observed that mutation of K44, an ATP-binding lysine conserved in all protein kinases, to methionine renders IKK2 inactive towards specific phosphorylation of S32 or S36 of IκBα, but not non-specific substrates. These observations highlight an unusual evolution of IKK2, in which autophosphorylation of tyrosine(s) in the activation loop and the invariant ATP-binding K44 residue define its signal-responsive substrate specificity ensuring the fidelity of NF-κB activation.

Introduction:

Inflammatory or pathogenic signals trigger precisely regulated induction of the transcription factor NF-κB in metazoans(Hoffmann and Baltimore, 2006). This process depends upon the upstream activation of the Inhibitor of κB Kinase-complex (IKK-complex), comprising two catalytic subunits, IKK1 (also known as IKKα) and IKK2 (or IKK2β), and an essential regulatory scaffolding protein, NEMO (IKK□)(DiDonato et al., 1997; Rothwarf et al., 1998; Zandi et al., 1997). IKK2 activity is maintained at a very low basal level in resting cells(Ghosh and Karin, 2002; Hacker and Karin, 2006; Hinz and Scheidereit, 2014; Liu et al., 2012). Upon activation, IKK2 phosphorylates the N-terminus of IκBα (Inhibitor of κBα) protein specifically at two Serine residues (S32 and S36) marking it for ubiquitinylation-mediated proteasomal degradation (Figure 1A). This liberates NF-κB to execute its gene expression program(Hayden and Ghosh, 2008; Hinz and Scheidereit, 2014; Karin and Ben-Neriah, 2000; Scheidereit, 2006). Mutation of both S32 and S36 to alanine residues converts IκBα into a non-phosphorylatable super-repressor of NF-κB(Brown et al., 1995; Lin et al., 1995).

Furthermore, IKK possesses exquisite specificity for these two serines, and it fails to phosphorylate IκBα when S32 and S36 are mutated even to another phosphorylatable residue, threonine(DiDonato et al., 1997).

IKK2 is an essential Ser/Thr kinase that ensures the activation of a particular signaling cascade - NF-κB, with high fidelitydespite its reported pleiotropy in other contexts(Antonia et al., 2021; Schröfelbauer et al., 2012; Schrofelbauer and Hoffmann, 2011). IKK2 is a multidomain protein consisting of a kinase domain (KD) followed by a Ubiquitin-like domain (ULD) and the scaffold dimerization domain (SDD) (Figure 1B). IKK2 toggles between inactive and active states based on the phosphorylation status of two serine residues (S177 and S181; S176 and S180 in the case of IKK1) within its activation loop (activation loop) in the KD(Huse and Kuriyan, 2002; Liu et al., 2013; Polley et al., 2013; Xu et al., 2011). Replacement of these two serines with phospho-mimetic glutamate residues (S177E, S181E; henceforth EE) renders the kinase constitutively active. IKK2 is reported to be primed through phosphorylation at S177 by the upstream kinase TAK1 that leads to auto-phosphorylation at S181, thus rendering the kinase fully active in cells(Zhang et al., 2014). However, oligomerization upon association with NEMO, in the presence of linear or Lys-63 linked poly-ubiquitin (Ub) chains or at a high concentration of IKK2, also enables *trans* auto-phosphorylation at S177 and S181(Chen, 2012; Du et al., 2022; Ea et al., 2006; Polley et al., 2013). It was also shown that NEMO not only helps in the activation of the IKK-complex, but also ensures that the IKK-activity is well directed towards IκBα in the inhibitor bound transcriptionally inactive NF-κB (NF-κB: IκBα complex)(Schröfelbauer et al., 2012). Activated IKK2 phosphorylates IκBα specifically at residues S32/S36 and the C-terminal SDD of IKK2 (residue range 645-756) is necessary for this(Shaul et al., 2008). Other sites of IκBα, but not S32/S36, can be phosphorylated by various kinases(Barroga et al., 1995; Tergaonkar et al., 2003). The role of IκBα-phosphorylation at sites other than the signal responsive S32/S36 phosphorylation in NF-κB activation and signaling is elusive. These findings underscore the ability of IKK2 to function specifically in guaranteeing rapid NF-κB activation in canonical signaling. It is

however, still not fully understood how IKK2 achieves its exquisite specificity towards S32/S36 of IκBα to mark it for proteasomal degradation that liberates active NF-κB dimers.

Here we report an in-depth analysis of the catalytic features of IKK2 that revealed that IKK2 undergoes multisite autophosphorylation and can phosphorylate its own tyrosine residue(s) in addition to its own serines or the serines of its substrate IκBα, i.e., IKK2 possesses dual specificity. This phosphorylation at tyrosine residue(s) is autocatalytic. This phosphorylation at tyrosine residues is dependent upon the prior activation of IKK2 via activation loop S177/S181 phosphorylation, and critical to phosphorylation of signal responsive S32/S36 of IκBα. Mutation of Y169 of IKK2 to phospho-ablative phenylalanine severely compromised phosphorylation of IκBα at S32. Mutation of Y188 to phenylalanine rendered the kinase practically inactive *in vitro*. IKK2 activity towards signal responsive S32/S36 of IκBα was severely compromised in MEF cells reconstituted with these two mutant IKK2s in response to treatment with TNFα. We also observed that mutation of the conserved ATP-interacting residue K44 in IKK2 to methionine leads to a loss of tyrosine as well as S177,S181 auto-phosphorylation activity of the kinase along with its ability to phosphorylate S32/S36 of IκBα. Interestingly, IKK2 K44M retained non-specific kinase activity. Furthermore, we observed that, after auto-phosphorylation at tyrosine, IKK2 can phosphorylate IκBα in the absence of exogenous supply of ATP, as long as ADP is present in the reaction. Overall, our results reveal unique, and likely transient, autophosphorylated intermediates of IKK2 that appear to be critical in relaying phosphoryl group(s) specifically to S32/S36 of IκBα in presence of ADP, thus ensuring fidelity of NF-κB activation. Recent reports in other kinases indicate that multisite (auto)phosphorylation is a major determinant in regulating function of respective kinases and regulation exerted by those kinases. Our study adds another layer of regulation and critical nature of such autophosphorylation that plays a significant biological role in metazoans.

Results:

IKK2 undergoes auto-phosphorylation at uncharacterized sites:

Signal-induced phosphorylation of activation loop Ser177/Ser181 marks the general activation of IKK2 (Figure 1B). Phosphorylation of several other serines located within the flexible C-terminal region of IKK2, spanning amino acid 701 to the end, has also been reported (Figure 1B)(Delhase et al., 1999). Hyperphosphorylation of these C-terminal sites down-regulates IKK2 activity in cells. It was also reported earlier that, ectopically overexpressed IKK2 is capable of autophosphorylating these two serines in the activation loop in *trans* even in the absence of an activating physiological signal. Indeed, recombinantly purified FL IKK2WT is capable of autophosphorylation *in vitro* when incubated with γ^{32}P-ATP that increases with the time of incubation (Figure 1C). The spread-out of slower migrating phospho-IKK2 band likely indicates phosphorylation of the protein at multiple sites. We also observed that autophosphorylation of IKK2 occurred irrespective of the presence of its cognate binding partner NEMO and *bonafide* substrate IκBα (Figure 1D). To confirm that this phosphorylation of IKK2 was indeed autophosphorylation and not due to an unrelated kinase copurified with IKK2, we generated a K44M mutant of full-length IKK2 where the ATP-binding invariant lysine residue conserved in STYKs was mutated to methionine, that is expected to greatly reduce or eliminate the kinase activity. An *in vitro* kinase assay using this mutant along with the WT kinase using γ^{32}P-ATP as the phosphor-donor confirmed that the IKK2 K44M lacked both IκBα (substrate) and autophosphorylation activities (Figure S1A). That these phosphorylations were indeed autophosphorylation was further supported by another *in vitro* radioactive kinase assay performed in the presence or absence of an IKK-specific ATP-competitive inhibitor, Calbiochem Inhibitor VII (Figure 1E). Purification status of recombinant FL IKK2 WT and FL IKK2 K44M proteins used in this study are shown in Figure S1B.

Next, we used different versions of the IKK2 protein where all previously known phosphorylation sites were lacking: Ser177 and 181 were mutated to phosphor-mimetic Glu (EE; this version of IKK2 is known to be constitutively active (Zandi et al., 1998)), and the C-terminal serine-rich region was truncated to different extents. The shortest construct, Δ664EE that entirely lacked the flexible C-terminus (670-756) was further subjected to limited

proteolysis using trypsin to eliminate residues, if any, from the flexible ends of the enzymes and this trypsin-treated IKK2 was purified prior to *in vitro* kinase assays. Each of these constructs was active in phosphorylating itself and the substrate IκBα (Figure 1F). The occurrence of autophosphorylation despite the absence of activation loop serines and serines within the C-terminus strongly suggested the presence of hitherto uncharacterized sites of autophosphorylation in IKK2.

Auto-phosphorylation of IKK2 reveals its dual specificity:

IKK2 is known as a *bonafide* Ser/Thr kinase that undergoes autophosphorylation. In the previous section, we found that IKK2's autophosphorylation activity might extend beyond the previously characterized site(s). We asked if it is a dual specificity kinase. To test if Tyr residues can undergo auto-phosphorylation in addition to Ser, IKK2 incubated with Mg^{2+}-ATP for various time periods was probed with antibodies that specifically recognize activation loop serines of IKK2 (Figure 2A, upper panel) or phospho-tyrosine residues (Figure 2A, middle panel). Unexpectedly, we observed *de novo* auto-phosphorylation of IKK2 on tyrosine residues along with the anticipated auto-phosphorylation of activation loop serines. It may be noted that autophosphorylation activation loop-S177/181 also increased with time, indicating inhomogeneous and incomplete phosphorylation of activation loop-S177/181 in the recombinant IKK2 when purified from Sf9 cells. We tested another phospho-tyrosine specific antibody to further substantiate this *de novo* tyrosine autophosphorylation of IKK2. It confirmed that detection of *de novo* phosphotyrosine on IKK2 was independent of the source of the antibody used (Figure 2B). The tyrosine auto-phosphorylation was abolished in the presence of an IKK-specific inhibitor, Inhibitor VII (Figure 2C). A similar assay was performed to monitor the phospho-tyrosine level in IKK2 as a function of urea concentration. This revealed the detrimental effects of urea on tyrosine autophosphorylation of IKK2 at concentrations beyond 1M (Figure S2A). A more sensitive assay with γ^{32}P-ATP as the phospho-donor also indicated that urea concentrations beyond 1M inhibited both auto-phosphorylation (pan-phosphorylation) and substrate (IκBα) phosphorylation (Figure S2B). Furthermore, the IKK2-

K44M mutant (kinase inactivating) did not display any tyrosine autophosphorylation when incubated with ATP unlike WT IKK2 (Figure 2D). These results confirm the novel tyrosine phosphorylation ability of IKK2, demonstrating its dual specificity to both its own Ser and Tyr residues. We also observed that activity of IKK2 towards S32 and S36 of IκBα and its own tyrosine residue(s) were affected similarly when the kinase assays were performed in the presence of various kinase inhibitors, both general (AMPPNP and Staurosporine) and IKK-specific (MLN-120B, TPCA, Inhibitor VII) (Figure S2C). These observations confirm that canonical activity of IKK2 towards S32 and S36 of IκBα, and towards its own tyrosine residues are mediated by the same active site.

Next, we checked the requirement of the C-terminal NEMO binding domain (NBD) for autocatalytic dual specificity. Constructs of various truncations (lacking NBD) were capable of phosphorylating itself on tyrosine residue(s), and phosphorylating IκBα at signal-responsive S32 and S36 (Figure 2E). Next, we assessed the autocatalysis at Ser and Tyr by IKK2 using a constitutively active NBD-truncated version of IKK2 (IKK2$^{\Delta 664}$EE). As anticipated, the protein was recognized by monoclonal phospho-serine antibody with or without fresh ATP-treatment; however, phospho-tyrosine antibody recognized it strongly only upon fresh ATP-treatment (Figure 2F).

Next, we asked if phosphorylation of activation loop S177/S181 was necessary for this dual specificity of IKK2. To this end, we purified the S177A, S181A (AA; non-phosphorylatable activation loop) phospho-ablative mutant of IKK2, and checked its tyrosine autophosphorylation activity. We found that the IKK2 AA mutant lacked tyrosine autophosphorylation activity (Figure 2G) in an *in vitro* kinase assay. It suggests that activation loop S177/S181 serine phosphorylation is essential in conducting dual specificity in IKK2. Indeed, the IKK2 AA mutant was incapable of phosphorylating S32/36 of IκBα as well (Figure S2D) in an *in vitro* kinase assay.

IKK2 autophosphorylation is critical to specificity of IκBα phosphorylation:

As mentioned earlier, it was long known that activation loop-serine phosphorylation was necessary for IKK-activation; we have now established that IKK2 phosphorylates itself on tyrosine residue(s) in addition to activation loop-serines. We wanted to further understand the significance of IKK2 autophosphorylation in the phosphorylation of S32/S36 of IκBα. It is known that disruption of a universal salt bridge mediated by the ATP-binding Lys (K44 in IKK2) is detrimental for kinase activity. However, it is not known if disruption of this salt bridge has any bearing on substrate specificity of EPKs. During our investigation, we noted unusual behavior in the IKK2-K44M mutant. We had noticed earlier that IKK2-K44M was incapable of *de novo* autophosphorylation on tyrosine residues (Figure 2D). It also failed to phosphorylate itself on the activation loop Ser177 and 181 (Figure 3A). Interestingly, IKK2-K44M phosphorylated full-length WT IκBα robustly albeit much less efficiency than WT IKK2 (Figure 3B) in a radioactive *in vitro* kinase assay. IKK2-K44M also showed a minor auto-phosphorylation activity compared to WT IKK2 in the absence of substrate (Figure 3B). We performed a similar kinase assay using full-length WT IκBα where cold ATP was used as the phosphate donor, and phosphorylation status of IκBα at S32, S36 was monitored by immunoblotting. It revealed that IKK2-K44M is unable to phosphorylate S32/S36 of IκBα (Figure 3C). Since radioactive kinase assays report pan-phosphorylation of a substrate (Figure 3B), it possibly reflects phosphorylation of the PEST region of FL IκBα. We additionally compared IKK2-K44M with WT IKK2 using radioactive kinase assay with both FL IκBα WT and FL IκBαAA substrates in the absence or presence of Inhibitor VII. As anticipated, FL IκBα was phosphorylated much more efficiently than FL IκBαAA by WT IKK2, and phosphorylation was practically abolished in the presence of 10 μM Inhibitor VII (Figure 3D). In contrast, IKK2-K44M phosphorylated FL IκBαAA more efficiently than FL IκBα, and reduction in the presence of inhibitor VII was strikingly less (Figure 3D). It indicates that IKK2-K44M, despite retaining non-specific kinase activity, lost phosphorylation activity towards S32, S36 of the *bona fide* substrate IκBα. We subjected 100ug of FL IKK2 K44M protein used in the above studies to

LC-MS/MS analysis, which did not detect any contaminating kinase from Sf9 cells. It is noteworthy that an equivalent K to M mutation in Erk2 also did not abolish the basal activity, but rather retained ~5 % of it(Robbins et al., 1993). The above set of experiments strongly suggest that IKK2-autophosphorylation is critical for its substrate specificity.

Tyrosine phosphorylation is critically important for IKK2 activity:

A number of earlier studies indicated that phosphorylation of IKK2 on Y169, Y188 and/or Y199 to be critical for its function(Darwech et al., 2010; Meyer et al., 2013). Our mass spectrometric analyses identified multiple tyrosine residues to be phosphorylated, e.g., Y169, Y188, Y199, Y325 (data not shown). We compared available structural models of human IKK2 (PDB ID: 4KIK, 4E3C) to investigate whether tyrosine phosphorylation within the activation loop could be supported based on its structural features(Liu et al., 2013; Polley et al., 2013). The structure of IKK2 dimer is asymmetric in that the activation loop of one monomer is largely disordered while that of the other monomer is mostly ordered (PDB ID: 4KIK)(Liu et al., 2013). In the active monomers S177 and S181 are clearly observed. In these active state conformers, the position and conformation of Tyr169 appears to be well-poised for accepting a phosphate from ATP (Figure S4A) intramolecularly. A superposition of IKK2 with a pseudo-substrate-bound PKA shows that the hydroxyl of Tyr169 in IKK2 projects toward the γ-phosphate of ATP similarly to the serine hydroxyl on the PKA inhibitor pseudo-substrate(Knighton et al., 1991; Nolen et al., 2004) (Figure S4A & B). Interestingly, Y169 is the DFG+1 (DLG in case of IKK2 and IKK1) residue while Y188 (equivalent to Y204 of PKA) is located at the end of activation loop prior to the conserved APE motif (Figure 4A and 4B). It was previously established that the DFG+1 position is crucial for defining the substrate specificity of a kinase(Chen et al., 2014). Y188 counterpart Y204 of PKA is reported to allosterically modulate PKA activity by altering its conformational entropy(Ahuja et al., 2017; Yang et al., 2005). We further focused our attention to Y169 and Y188 as they are located in the activation loop of the kinase.

To test the effect of phosphorylation at Y169 and Y188, we generated Y169F and Y188F mutants of IKK2. Radioactive *in vitro* kinase assays using recombinant purified $IKK2^{FL}$-

Y188F and IKK2^{FL}-Y169F mutants revealed a drastic reduction in the activity of IKK2 (Figure 4C). Since the DFG+1 residue in kinases (Y169 in IKK2) is known to dictate its specificity, we created different mutants of the IκBα substrate where S32 and S36 were singly and independently altered to either alanine (phosphoablative) or glutamic acid (phosphomimetic) residues. Kinase activity of IKK2-Y169F was monitored in an *in vitro* radioactive kinase assay using WT as well as mutant IκBα. Mutation of S36 to either Ala or Glu drastically reduced the phosphorylation signal of IκBα while that for the S32A/E mutants were minimally affected (Figure 4D). This suggests that the presence of Tyr (and possibly its phosphorylation) is critically important for signal-responsive phosphorylation of IκBα.

Next, we tested the consequence of Y169F and Y188F mutants on the pro-inflammatory signal-induced IKK activity in cells. We reconstituted IKK2 knock-out mouse embryonic fibroblast (*ikk2*$^{-/-}$ MEF) cells with WT, Y169F and Y188F mutants of IKK2, and measured signal-induced activation of IKK2 upon TNF-α treatment. IKK2 activity is significantly reduced in Y169F and nearly abolished in Y188F (Figure 4E**)**. Interestingly, phosphorylation of activation loop serines of the less active Y169F mutant was only marginally defective (Fig. 4F). This suggests that activation loop phosphorylation is necessary but not sufficient for IKK2 to become fully active. Together, these results suggest an unreported communication between the phosphorylation of Y169 of IKK2 and that of S32 of IκBα.

Structural analyses of IKK2 autophosphorylation:

To get a more comprehensive picture, it is necessary to analyze at least three phosphorylated states of IKK2: unphosphorylated (UnP-IKK2), phosphorylated at S177 and S181 (p-IKK2), and phosphorylated at Y169, S177 and S181 (P-IKK2). We took advantage of computational approaches using molecular dynamic (MD) simulations and flexible molecular docking (see methods).[43–50] MD simulation was performed for 200ns for each of these three states of IKK2, unphosphorylated and phosphorylated. Phosphorylation at S177, S181 increased the stability of the kinase, which was further increased by the phosphorylation at Y169 as evidenced by a gradual decrease in the total energy (Figure 5A). A striking

enhancement in stability of IKK2 upon this auto-phosphorylation is reflected in the change of Tm from ~ 40 °C to ~ 50 °C in differential scanning calorimetry (DSC) scans in the presence of ADP and ATP (Figure S4A). This behavior supports our observation in MD simulation, and tallies with increased solubility of IKK2 observed after auto-phosphorylation that was essential for its successful crystallization.(Polley et al., 2013)

Interestingly, RMSD values increased with more phosphorylation (Figure 5B) despite phosphorylation-induced stabilization, P-IKK2 showed the highest RMSD followed by p-IKK2 and UnP-IKK2. We found that, phosphorylation at S177, S181 and S177, S181, Y169 induced distinct structural alteration in the KD when compared with the unphosphorylated version (Figure 5C, models shown separately in Figure S4B). Careful analyses of the trajectory of RMSF values for these three states revealed that, different regions of the kinase domain had different RMSF values in different phosphorylated states (Figure S4C). We observed that, while the glycine-rich loop and the αC-helix in p-IKK2 were situated in a manner reminiscent of an active kinase (Figure S4D), those in UnP and P-IKK2 were placed very differently. In fact, helix αC was found to be distorted in P-IKK2, that is unlikely to support canonical phosphotransfer from ATP. Activation segment/loop (activation loop) in these three differently phosphorylated states adopted conformations distinct from each other. activation loop in the UnP model was displayed out and moved closer to the tip of the C-lobe, whereas activation loop in p-IKK2 and P-IKK2 moved inwards and adopted conformations closer to the N-lobe. The formation of the proper R- and C-spines in p-IKK2 confirmed its active form (Figure 5D). p-IKK2 KD also exhibited other canonical features of an active kinase, viz., a salt bridge between K44 and E61 (K72, E91 in PKA, respectively), 'DFG in' (DLG here) conformation. Next, we docked ATP onto the p-IKK2 structure (ΔG = -10.64 kcal/mol) using a flexible docking protocol (see methods). The ATP and its phosphate groups exhibited a pose (Figure S4D) very similar to that in the PKA structure (PDB ID: 1ATP), and the terminal phosphate was in close proximity to Y169-OH making autophosphorylation of Y169 highly plausible (Figure 5E). Further analyses of the ATP-bound p-IKK2 structure confirm that presence of ATP helped the

R and C-spine form the desired continuum of an active kinase (Figure 5F). Superposition of the ATP from the p-IKK2 on P-IKK2 indicated that the narrowing of ATP-binding pocket in P-IKK2 may lead to rejection of ATP emanating from severe clashes between the glycine-rich loop and ATP (Figure 5G). Furthermore, the R-spine in P-IKK2 was not continuous (Figure 5H), wherein M65 (L95 in PKA) of the four conserved residues were located at a position far away from the rest of three residues that constitute the R-spine, and from the glycine rich loop. In addition, dynamic cross-correlation matrix (DCCM) or contact map of each structure suggests that specific phosphorylation events render the kinase display distinct allosteric changes at locations far from the phosphorylation sites themselves (Figure S4E).

ATP binding to p-IKK2 leads to autophosphorylation at Y169 generating P-IKK2 in an ADP bound state. Interestingly, the superposition of ADP (from the docked complex of p-IKK2 and ADP, ΔG = -9.88 kCal/mol, Figure 5I) onto the P-IKK2 structure confirmed that while P-IKK2 was unable to accommodate ATP in a manner similar to that in other known experimentally derived kinase structures, it could comfortably accommodate ADP into the ATP-binding cleft (Figure 5J). It may be noted that, p-IKK2 has higher affinity for ATP than ADP as indicated by their respective binding energy values. We speculate that ADP-bound P-IKK2 is an intermediate step where presence of as many phosphate groups in the activation loop and ADP in such a close proximity persuades the kinase to adopt a conformation that can withstand this high density of negative charges albeit risking the integrity of an active fold, and making some of those *de novo* phosphate groups transient in nature to return back to the p-IKK2 state to readily bind to ATP.

These structural observations suggest that it is possible for the residues within the flexible activation segment to undergo auto-phosphorylation and possibly render the kinase with a novel phospho-transfer activity without requiring ATP.

Freshly auto-phosphorylated IKK2 phosphorylates IκBα even in absence of ATP:

We observed phosphorylation of tyrosine residue(s) by WB or mass spectrometry only upon fresh ATP-treatment, indicating that tyrosines of purified IKK2 loses its phosphate group

(Eckhart et al., 1979). It may be noted that, we did not observe any density of phosphates on any of these residues in the human IKK2 crystal structure derived from ATP-treated protein sample (Polley et al., 2013). Of note, human IKK2 crystals grown with autophosphorylated IKK2 (PDB ID 4E3C) took about a month at 18-20°C before they were subjected to X-ray diffraction. This suggested an intriguing possibility that the phosphate linked to Tyr residue(s) may serve as a temporary phosphate-sink and could eventually be transferred to substrate IκBα. To test this possibility, we first allowed purified IKK2 to undergo auto-phosphorylation by incubating the excess kinase with limiting amounts of radiolabeled γ-^{32}P-ATP followed by two passes through desalting spin columns (40 kDa MW cut-off) to remove unreacted ATP. Nucleotide-free auto-phosphorylated IKK2 (P-IKK2) was incubated with IκBα either in absence of nucleotide or with newly added unlabeled nucleotides, and phosphorylation status of the substrate was subsequently monitored by autoradiography after resolving the reaction mixture on an SDS-PAGE (Figure 6A). Transfer of radiolabeled phosphate to IκBα was observed and the transfer was significantly enhanced in the presence of cold ADP (Figure 6B). Phosphorylation of IκBα did not significantly decrease in the presence of a high concentration of cold ATP. That addition of excess cold ATP did not reduce the extent of IκBα phosphorylation strongly suggests the transfer of ^{32}P-phosphate from ^{32}P-IKK2 to IκBα (Figure 6B) by a relay mechanism with or without involving ADP.

We undertook a different strategy to further confirm transfer of phosphate from the kinase (and not ATP) to the substrate. We auto-phosphorylated IKK2^{FL}-WT with excess cold ATP and removed the unreacted ATP from the reaction mixture using size-exclusion chromatography on a Superdex200 column (Figure 6C). P-IKK2 eluted at fractions corresponding to MW between 670 and 158 kDa, i.e., much larger than free ATP (Figure 6D). This P-IKK2 protein was incubated with FL IκBα either in presence or absence of ADP for different time periods. A similar reaction in presence of ATP instead of ADP was performed as a positive control. Phosphorylation of S32 and S36 was efficient in presence of 10 and 50 μM ADP but absent when ADP was absent in the reaction mixture. Phosphorylation of IκBα

in the presence of 50 μM ATP was significantly more robust as anticipated (Figure 6E). The minor detection of IκBα phosphorylation in absence of ADP in the radioactive assay and lack of it in the cold immunoblotting assay (compare lanes marked with vertical arrows in Figures 6B and 6F) may indicate higher sensitivity of the radioactive assay. The need of ADP in phosphotransfer prompted us to consider whether the ADP was contaminated with a trace amount of ATP. ESI-MS analysis of 50 μM ADP did not detect any peak corresponding to ATP (Figure S5A). Dependence of IκBα phosphorylation on ADP could raise another possibility if microscopic reversibility generated ATP from ADP in the active site of the kinase. To this end, we employed TLC-based analysis to detect generation/presence of ATP in a similar setting as described in Fig. 5A-B which revealed that no detectable ATP was present in the system (Figure S5B).

Phosphotransfer from P-IKK2 is critical to fidelity and specificity of IκBα phosphorylation:

We next tested if phosphotransfer is restricted only to the N-terminal signal responsive S32/S36 or to serines/threonines of the PEST domain as well. Radioactive kinase assay as described earlier was performed with full-length WT and mutant S32A, S36A (AA) IκBα as the phosphate recipient. Phosphate group(s) of P-IKK2 was not transferred to full-length IκBα AA which retains the serines and threonines within its PEST domain (Figure 7A), indicating phosphotransfer only to the N-terminal serines of IκBα. We also tested the effect of AMPPNP, an unhydrolyzable analogue of ATP, on the phosphotransfer, and found no inhibitory effect irrespective of the presence of ADP. This suggests adenine nucleotides poising the kinase for phosphotransfer (Figure 7A). A recent report proposed that IKK2 phosphorylates IκBα at S32 followed by S36 following a single binding event and that phosphorylation of S32 increases the phosphorylation rate of S36(Stephenson et al., 2022). Based on our results and other evidence, we propose that IKK2 phosphorylated at S177/S181 undergoes autophosphorylation on tyrosine residues in its activation loop area that serves as a phosphoenzyme intermediate to transfer phosphate group from IKK2 to S32 that enhances

the rate of second site (S36) phosphorylation (Figure 7B). For the second site phosphorylation ATP serves as the phosphate donor.

Discussion:

Phosphorylation of substrates by protein kinases is regulated in various ways(Cullati et al., 2022; Sang et al., 2022). IKK2, a kinase central to inflammation, phosphorylates serine residues of its primary substrate IκBα with γ-phosphate of ATP. Here, we report multiple intriguing properties of IKK2 that provide specificity to its substrate phosphorylation. These include: 1) dual specificity that entails autophosphorylation of tyrosine residues of IKK2, in addition to known auto-phosphorylation at activation loop serines; 2) relay of phosphate to substrate IκBα from auto-phosphorylated IKK2 (P-IKK2) and 3) loss of specificity of the kinase due to disruption of a universally conserved salt bridge (mediated by K44).

Ser/Thr/Tyr family of eukaryotic protein kinases transfer γ-phosphate of ATP directly to substrate, in general to S, T and Y residues(Cohen, 2002; Fischer and Krebs, 1955; Hunter, 1991; Krebs and Fischer, 1955; Nolen et al., 2004). Histidine kinases (in prokaryotes and in some lower eukaryotes) however shuttles the γ-phosphate to Asp residue on a response regulator (RR) substrate through a phospho-His intermediate(Borkovich and Simon, 1990; Gao and Stock, 2009; Hunter, 2022; Kalagiri and Hunter, 2021; Laub et al., 2007; Robbins et al., 1993). Our present analyses of eukaryotic protein kinase IKK2 revealed its surprising property in which IKK2 phosphorylated at activation loop-serines (S177/S181) could be further auto-phosphorylated by ATP at multiple other residues yielding another form (P-IKK2) (Figure 7B). This marks IKK2 as an autocatalytic dual-specificity kinase rather than a prototype S/T kinase. This multisite phosphorylated form of IKK2 (P-IKK2) could transfer phosphate(s) to substrate IκBα in presence of ADP without requiring exogenous supply of fresh ATP, hinting at an unusual property of IKK2 acting possibly as a phosphate-sink. It is possible that phospho-tyrosines residues of IKK2 act as this sink. The Y169 located at the DFG+1 (DLG in IKK2) position is unique only to IKK1 and IKK2, and is absent even in close mammalian homologues such as IKKε and TBK1. Interestingly, neither IKKε nor TBK1 can phosphorylate IκBα at S32

and S36, *in vitro* or *in vivo*(Larabi et al., 2013; Tu et al., 2013). A recent report also indicated the role of DFG+1 residue in differentiating Ser versus Thr residues(Chen et al., 2014). These observations hinted to an involvement of Y169 in substrate selectivity. Indeed, our experimental data suggests a pivotal role of Y169 in phosphorylating S32 of IκBα both *in vitro* and *ex vivo* (Figure 4D & 4E). It is worthwhile to note that, a phosphoablative mutation at S32 in IκBα to Ile (S32I) is associated with ectodermal dysplasia and T-cell immunodeficiency in patients(Courtois et al., 2003; Mooster et al., 2015). More interestingly, the placement of Y169 in the kinase active site makes it amenable to a phosphorylation-dephosphorylation cycle, suggesting its possible role both in phosphotransfer and substrate specificity. Mutation of Y188, a conserved tyrosine, to non-phosphorylatable phenylalanine abolished the kinase activity of IKK2 *in vitro* as well as in MEFs upon TNF-treatment (Figure 4C & 4E). The placement of Y188 indicates that its mutation will be detrimental to the structural fold of kinase, thus it is unclear if or how Y188 plays a role in the phosphotransfer. Since phosphotransfer to S32, S36 of IκBα is observed with auto-phosphorylated IKK2 EE, transferred phosphates are not from S177 or S181. Kinase domain autophosphorylation is known to regulate function of other kinases as well, e.g., autophosphorylation at T220 greatly influenced both the activity and substrate specificity of CK1(Cullati et al., 2022).

The strength of input signal, level of IκBα degradation, and NF-κB activation correlate with the amplitude, duration, and kinetics of IKK activity(Behar and Hoffmann, 2013; Cheong et al., 2006). This digital (all-or-none) activation profile of NF-κB appears to be due to rapid activation and inactivation of IKK2. IKK targets multiple substrates *in vivo*; however, the rapid activation of NF-κB is regulated primarily by IκBα. How IKK specifically selects IκBα for phosphorylation is unclear, although NEMO is reported to direct the kinase activity of IKK2 specifically towards IκBα(Schröfelbauer et al., 2012). We observe that P-IKK2 could transfer phosphate(s) specifically to the S32/S36 of IκBα, and not to other sites (such as the PEST sequence of IκBα) (Figure 6B, 6E and 7A). We surmise if transiency of multisite phosphorylated IKK2 (P-IKK2) underlie this activation-inactivation events during signal

response. It is possible that regulatory system of IKK2 is somewhat analogous the two-component histidine kinase-effector systems in prokaryotes that show a threshold activation response(Bhate et al., 2015; Lamarche et al., 2008; Laub and Goulian, 2007). It is noteworthy that, transfer of a phosphate moiety directly from pHis is energetically much more probable than that from a pTyr, unless it is an enzymatic process which is likely the case for IKK2:IκBα system.

Tyrosines in activation loop of IKK2 are previously reported to undergo signal-induced phosphorylation in cells. These modifications were proposed to be mediated by a tyrosine kinase although there is no evidence of a specific tyrosine kinase(Meyer et al., 2013; Otero et al., 2008; Rieke et al., 2011). Several members of the Ser/Thr kinase family undergo tyrosine phosphorylation and these kinases employ diverse mechanisms for auto-phosphorylation(Bhattacharyya et al., 2006; Ge et al., 2002; Lochhead, 2009; Lochhead et al., 2006, 2005; Tigno-Aranjuez et al., 2010).

The phosphotransfer from P-IKK2 to IκBα monitored here is detection of a single turnover event in absence of the phosphate donor, ATP (Figure 6B). Phosphorylation on IKK2 occurs at multiple sites, and not every phosphorylated residue in P-IKK2 expected to transfer its phosphate to IκBα. There is more than one type of phosphorylated residues in P-IKK2 distributed over the length of the kinase, arguably with differential stability wherein only a fraction of the total pool can be relayed. In addition, it is likely that the phosphorylated IKK2 in the bulk harbors a non-homogenous pool where differently phosphorylated species of the kinase are present, and are indistinguishable in our assay schemes. Another intriguing feature of phosphorelay in IKK2 is IKK2's dependence on ADP (Figure 6B & 6E). It was also observed that, the generic kinase inhibitor AMPPNP (unhydrolyzable ATP analogue) failed to inhibit phosphor-transfer from IKK2 (Figure 7A) and IκBα phosphorylation (Figure S2C). Taken together, we surmise that presence of ADP or AMP-PNP help IKK2 attain a conformational state poised for phosphorylating S32/36 of IκBα even in absence of fresh exogenous ATP. Similar phenomenon was reported for IRE1, where ADP was found to be a more potent

stimulator of its ribonuclease activity and that AMPPNP could also potentiate this activity in IRE1(Lee et al., 2008; Sidrauski and Walter, 1997).The list of Ser/Thr kinase family proteins that undergo tyrosine phosphorylation is growing that employ diverse mechanisms for auto-phosphorylation(Bhattacharyya et al., 2006; Ge et al., 2002; Lochhead, 2009; Lochhead et al., 2006, 2005; Tigno-Aranjuez et al., 2010). The most notable example of this dual specificity are DYRK and GSK3β. However, the role of Tyr-phosphorylation in DYRK/GSK3β is not related to that in IKK2, nor does it render DYRKs/ GSK3β capable of relaying phosphates to the substrates. To the best of our knowledge the only other reported example of an EPK, though atypical, transferring phosphate through a phosphoenzyme intermediate is MHCK of *Dictyostelium discoideum*(Ye et al., 2010).

Our study reveals tyrosine auto-phosphorylation in IKK2 and indicates that consequences of Ser and Tyr autophosphorylations in dual-specific IKK2 are distinct. Moreover, the crucial tyrosine residues are positioned in such a manner that some that are amenable to auto-phosphorylation are essential for substrate phosphorylation. Most surprisingly, the tyrosine-linked phosphate groups can be transferred by a relay mechanism to specific serines in IκBα, an event reminiscing phospho-relay in two-component systems prevalent in prokaryotes and some lower eukaryotes. Our study also reveals the role of K44 of IKK2 in auto-phosphorylation and thus in specific phosphorylation of S32, S36 of IκBα, although the mutant kinase retains its non-specific kinase activity. It may be noted that, while a monomeric version of IKK2 (devoid of NBD and large portion of the dimeric interface in the SDD) still retained its specificity for the N-terminal serines of IκBα(Hauenstein et al., 2014), while a shorter construct containing only the KD and ULD lacked this specificity that phosphorylated the PEST domain like CK2(Shaul et al., 2008). It requires further investigation to determine if a structural state of IKK2, perhaps through a different modification or through binding to another protein, allow it to phosphorylate substrates relatively non-specifically.

In all, it is intriguing how the gateway to the activation of NF-κB is regulated through unique phosphorylation events in IKK2 (Figure 7C). It appears that a multi-layered fail-safe

mechanism is devised to tightly control NF-κB activation. Firstly, in absence of upstream signals IKK-complex is unable to phosphorylate Ser 32,36 of IκBα efficiently thereby keeping check on the aberrant and untimely activation of NF-κB. Upon encountering proinflammatory cues, cells need to activate NF-κB immediately and efficiently, i.e., IKK needs to be activated and phosphorylate Ser 32,36 of IκBα. NEMO warrants IKK-activation and ensures that the IKK-complex specifically chooses IκBα from a large pool of substrates of IKK2. IKK2 is designed in such a manner that it phosphorylates itself at activation loop-tyrosines when activated, such that phosphate group(s) can be relayed directly to Ser32,36 of IκBα with great fidelity, thus leaving little chance of a misconstrued signaling event thereby confirming NF-κB activation (Figure 7C). Our discovery might also present the beginning of a new aspect in eukaryotic cell-signaling by EPKs and provide a foundation for mechanistic studies of an intriguing phospho-transfer reaction that helps accomplish the desired specificity. To the best of our knowledge, it is the first report, apart from MHCK of *Dictyostelium discoideum* (an atypical EPK), to suggest that a metazoan EPK confirms its specificity through the formation of a phosphoenzyme intermediate.

Methods summary:

Protein purification, auto-phosphorylation assay, immunoprecipitation coupled kinase assay, phosphotransfer assay and other experiments have been described in details in the supplementary document.

Acknowledgement:

We thank Tony Hunter (Salk Institute) for commenting on the work. Authors also thank members of Polley lab (BI) and Ghosh Lab (UCSD) for their continuous support. This work was supported by an Intermediate Fellowship from the DBT Wellcome Trust India Alliance (IA/I/15/1/501852) & intramural funding from Bose Institute to SP, NIH grant to GG (AI163327) and American Cancer Society grant RSG-08-287-01-GMC to TH. Biochemistry research at SDSU is supported in part by the California Metabolic Research Foundation. PB was supported by the graduate research fellowship from Bose Institute. SC acknowledges CSIR-

IICB for infrastructure support. AC acknowledges ICMR for post-doctoral Research Associateship [BMI/11(55)2022].

Author contribution:

SP, GG and TB designed experiments; PB, SP, TB & GG performed experiments. Computational analyses were performed by AC & SC. SP, GG, TB, PB, TH, SC and AC analyzed the results. SP wrote the manuscript with the help of PB, TB and AC in preparing figures and images. GG, TB, PB and TH edited/modified the manuscript. All authors commented on the manuscript.

Ethics declarations:

Competing interests: The authors declare no competing financial interests.

References:

1. Ahuja LG, Kornev AP, McClendon CL, Veglia G, Taylor SS. 2017. Mutation of a kinase allosteric node uncouples dynamics linked to phosphotransfer. *Proc Natl Acad Sci U S A* **114**:E931–E940. doi:10.1073/pnas.1620667114

2. Antonia RJ, Hagan RS, Baldwin AS. 2021. Expanding the View of IKK: New Substrates and New Biology. *Trends Cell Biol* **31**:166–178. doi:10.1016/j.tcb.2020.12.003

3. Barroga CF, Stevenson JK, Schwarz EM, Verma IM. 1995. Constitutive phosphorylation of I kappa B alpha by casein kinase II. *Proceedings of the National Academy of Sciences* **92**:7637–7641. doi:10.1073/pnas.92.17.7637

4. Behar M, Hoffmann A. 2013. Tunable Signal Processing through a Kinase Control Cycle: the IKK Signaling Node. *Biophys J* **105**:231–241. doi:10.1016/j.bpj.2013.05.013

5. Bhate MP, Molnar KS, Goulian M, DeGrado WF. 2015. Signal Transduction in Histidine Kinases: Insights from New Structures. *Structure* **23**:981–994. doi:10.1016/j.str.2015.04.002

6. Bhattacharyya RP, Reményi A, Good MC, Bashor CJ, Falick AM, Lim WA. 2006. The Ste5 scaffold allosterically modulates signaling output of the yeast mating pathway. *Science* **311**:822–826. doi:10.1126/science.1120941

7. Borkovich KA, Simon MI. 1990. The dynamics of protein phosphorylation in bacterial chemotaxis. *Cell* **63**:1339–1348. doi:10.1016/0092-8674(90)90429-i

8. Brown K, Gerstberger S, Carlson L, Franzoso G, Siebenlist U. 1995. Control of I kappa B-alpha proteolysis by site-specific, signal-induced phosphorylation. *Science* **267**:1485–1488. doi:10.1126/science.7878466

9. Chen C, Ha BH, Thevenin AF, Lou HJ, Zhang R, Yip KY, Peterson JR, Gerstein M, Kim PM, Filippakopoulos P, Knapp S, Boggon TJ, Turk BE. 2014. Identification of a major determinant for serine-threonine kinase phosphoacceptor specificity. *Mol Cell* **53**:140–7. doi:10.1016/j.molcel.2013.11.013

10. Chen ZJ. 2012. Ubiquitination in Signaling to and Activation of IKK. *Immunol Rev* **246**:95–106. doi:10.1111/j.1600-065X.2012.01108.x

11. Cheong R, Bergmann A, Werner SL, Regal J, Hoffmann A, Levchenko A. 2006. Transient IkappaB kinase activity mediates temporal NF-kappaB dynamics in response to a wide range of tumor necrosis factor-alpha doses. *J Biol Chem* **281**:2945–50. doi:10.1074/jbc.M510085200

12. Cohen P. 2002. The origins of protein phosphorylation. *Nat Cell Biol* **4**:E127–E130. doi:10.1038/ncb0502-e127

13. Courtois G, Smahi A, Reichenbach J, Döffinger R, Cancrini C, Bonnet M, Puel A, Chable-Bessia C, Yamaoka S, Feinberg J, Dupuis-Girod S, Bodemer C, Livadiotti S, Novelli F, Rossi P, Fischer A, Israël A, Munnich A, Le Deist F, Casanova J-L. 2003. A hypermorphic IkappaBalpha mutation is associated with autosomal dominant anhidrotic ectodermal dysplasia and T cell immunodeficiency. *J Clin Invest* **112**:1108–1115. doi:10.1172/JCI18714

14. Cullati SN, Chaikuad A, Chen J-S, Gebel J, Tesmer L, Zhubi R, Navarrete-Perea J, Guillen RX, Gygi SP, Hummer G, Dötsch V, Knapp S, Gould KL. 2022. Kinase domain autophosphorylation rewires the activity and substrate specificity of CK1 enzymes. *Mol Cell* **82**:2006-2020.e8. doi:10.1016/j.molcel.2022.03.005

15. Darwech I, Otero JE, Alhawagri MA, Abu-Amer Y. 2010. Tyrosine phosphorylation is required for IkappaB kinase-beta (IKKbeta) activation and function in osteoclastogenesis. *J Biol Chem* **285**:25522–25530. doi:10.1074/jbc.M110.121533

16. Delhase M, Hayakawa M, Chen Y, Karin M. 1999. Positive and Negative Regulation of IκB Kinase Activity Through IKKβ Subunit Phosphorylation. *Science* **284**:309–313. doi:10.1126/science.284.5412.309

17. DiDonato JA, Hayakawa M, Rothwarf DM, Zandi E, Karin M. 1997. A cytokine-responsive IκB kinase that activates the transcription factor NF-κB. *Nature* **388**:548–554. doi:10.1038/41493

18. Du M, Ea CK, Fang Y, Chen ZJ. 2022. Liquid phase separation of NEMO induced by polyubiquitin chains activates NF-kappaB. *Mol Cell* **82**:2415-2426 e5. doi:10.1016/j.molcel.2022.03.037

19. Ea CK, Deng L, Xia ZP, Pineda G, Chen ZJ. 2006. Activation of IKK by TNFalpha requires site-specific ubiquitination of RIP1 and polyubiquitin binding by NEMO. *Mol Cell* **22**:245–57. doi:10.1016/j.molcel.2006.03.026

20. Eckhart W, Hutchinson MA, Hunter T. 1979. An activity phosphorylating tyrosine in polyoma T antigen immunoprecipitates. *Cell* **18**:925–933. doi:10.1016/0092-8674(79)90205-8

21. Fischer EH, Krebs EG. 1955. Conversion of phosphorylase b to phosphorylase a in muscle extracts. *J Biol Chem* **216**:121–32.

22. Gao R, Stock AM. 2009. Biological Insights from Structures of Two-Component Proteins. *Annu Rev Microbiol* **63**:133–154. doi:10.1146/annurev.micro.091208.073214

23. Ge B, Gram H, Di Padova F, Huang B, New L, Ulevitch RJ, Luo Y, Han J. 2002. MAPKK-independent activation of p38alpha mediated by TAB1-dependent autophosphorylation of p38alpha. *Science* **295**:1291–1294. doi:10.1126/science.1067289

24. Ghosh S, Karin M. 2002. Missing pieces in the NF-kappaB puzzle. *Cell* **109 Suppl**:S81-96.

25. Hacker H, Karin M. 2006. Regulation and function of IKK and IKK-related kinases. *Sci STKE* **2006**:re13. doi:10.1126/stke.3572006re13

26. Hauenstein AV, Rogers WE, Shaul JD, Huang DB, Ghosh G, Huxford T. 2014. Probing kinase activation and substrate specificity with an engineered monomeric IKK2. *Biochemistry* **53**:2064–73. doi:10.1021/bi401551r

27. Hayden MS, Ghosh S. 2008. Shared principles in NF-kappaB signaling. *Cell* **132**:344–62. doi:10.1016/j.cell.2008.01.020

28. Hinz M, Scheidereit C. 2014. The IκB kinase complex in NF-κB regulation and beyond. *EMBO Rep* **15**:46–61. doi:10.1002/embr.201337983

29. Hoffmann A, Baltimore D. 2006. Circuitry of nuclear factor kappaB signaling. *Immunol Rev* **210**:171–86. doi:10.1111/j.0105-2896.2006.00375.x

30. Hunter T. 2022. A journey from phosphotyrosine to phosphohistidine and beyond. *Mol Cell* **82**:2190–2200. doi:10.1016/j.molcel.2022.05.007

31. Hunter T. 1991. Protein kinase classification. *Methods Enzymol* **200**:3–37. doi:10.1016/0076-6879(91)00125-g

32. Huse M, Kuriyan J. 2002. The conformational plasticity of protein kinases. *Cell* **109**:275–282. doi:10.1016/s0092-8674(02)00741-9

33. Kalagiri R, Hunter T. 2021. The many ways that nature has exploited the unusual structural and chemical properties of phosphohistidine for use in proteins. *Biochem J* **478**:3575–3596. doi:10.1042/BCJ20210533

34. Karin M, Ben-Neriah Y. 2000. Phosphorylation meets ubiquitination: the control of NF-[kappa]B activity. *Annu Rev Immunol* **18**:621–63. doi:10.1146/annurev.immunol.18.1.621

35. Knighton DR, Zheng JH, Ten Eyck LF, Xuong NH, Taylor SS, Sowadski JM. 1991. Structure of a peptide inhibitor bound to the catalytic subunit of cyclic adenosine monophosphate-dependent protein kinase. *Science* **253**:414–420. doi:10.1126/science.1862343

36. Krebs EG, Fischer EH. 1955. Phosphorylase activity of skeletal muscle extracts. *J Biol Chem* **216**:113–20.

37. Lamarche MG, Wanner BL, Crépin S, Harel J. 2008. The phosphate regulon and bacterial virulence: a regulatory network connecting phosphate homeostasis and pathogenesis. *FEMS Microbiol Rev* **32**:461–473. doi:10.1111/j.1574-6976.2008.00101.x

38. Larabi A, Devos JM, Ng SL, Nanao MH, Round A, Maniatis T, Panne D. 2013. Crystal structure and mechanism of activation of TANK-binding kinase 1. *Cell Rep* **3**:734–46. doi:10.1016/j.celrep.2013.01.034

39. Laub MT, Biondi EG, Skerker JM. 2007. Phosphotransfer profiling: systematic mapping of two-component signal transduction pathways and phosphorelays. *Methods Enzymol* **423**:531–48. doi:10.1016/S0076-6879(07)23026-5

40. Laub MT, Goulian M. 2007. Specificity in two-component signal transduction pathways. *Annu Rev Genet* **41**:121–45. doi:10.1146/annurev.genet.41.042007.170548

41. Lee KPK, Dey M, Neculai D, Cao C, Dever TE, Sicheri F. 2008. Structure of the dual enzyme Ire1 reveals the basis for catalysis and regulation in non-conventional RNA splicing. *Cell* **132**:89–100. doi:10.1016/j.cell.2007.10.057

42. Lin YC, Brown K, Siebenlist U. 1995. Activation of NF-kappa B requires proteolysis of the inhibitor I kappa B-alpha: signal-induced phosphorylation of I kappa B-alpha alone does not release active NF-kappa B. *Proceedings of the National Academy of Sciences* **92**:552–556. doi:10.1073/pnas.92.2.552

43. Liu F, Xia Y, Parker AS, Verma IM. 2012. IKK biology. *Immunol Rev* **246**:239–53. doi:10.1111/j.1600-065X.2012.01107.x

44. Liu S, Misquitta YR, Olland A, Johnson MA, Kelleher KS, Kriz R, Lin LL, Stahl M, Mosyak L. 2013. Crystal Structure of a Human IκB Kinase β Asymmetric Dimer. *J Biol Chem* **288**:22758–22767. doi:10.1074/jbc.M113.482596

45. Lochhead PA. 2009. Protein kinase activation loop autophosphorylation in cis: overcoming a Catch-22 situation. *Sci Signal* **2**:pe4. doi:10.1126/scisignal.254pe4

46. Lochhead PA, Kinstrie R, Sibbet G, Rawjee T, Morrice N, Cleghon V. 2006. A chaperone-dependent GSK3beta transitional intermediate mediates activation-loop autophosphorylation. *Mol Cell* **24**:627–633. doi:10.1016/j.molcel.2006.10.009

47. Lochhead PA, Sibbet G, Morrice N, Cleghon V. 2005. Activation-loop autophosphorylation is mediated by a novel transitional intermediate form of DYRKs. *Cell* **121**:925–936. doi:10.1016/j.cell.2005.03.034

48. Meyer AN, Drafahl KA, McAndrew CW, Gilda JE, Gallo LH, Haas M, Brill LM, Donoghue DJ. 2013. Tyrosine Phosphorylation Allows Integration of Multiple Signaling Inputs by IKKβ. *PLoS One* **8**:e84497. doi:10.1371/journal.pone.0084497

49. Mooster JL, Le Bras S, Massaad MJ, Jabara H, Yoon J, Galand C, Heesters BA, Burton OT, Mattoo H, Manis J, Geha RS. 2015. Defective lymphoid organogenesis underlies the immune deficiency caused by a heterozygous S32I mutation in IκBα. *J Exp Med* **212**:185–202. doi:10.1084/jem.20140979

50. Nolen B, Taylor S, Ghosh G. 2004. Regulation of Protein Kinases: Controlling Activity through Activation Segment Conformation. *Molecular Cell* **15**:661–675. doi:10.1016/j.molcel.2004.08.024

51. Otero JE, Dai S, Foglia D, Alhawagri M, Vacher J, Pasparakis M, Abu-Amer Y. 2008. Defective osteoclastogenesis by IKKbeta-null precursors is a result of receptor activator of NF-kappaB ligand (RANKL)-induced JNK-dependent apoptosis and impaired differentiation. *J Biol Chem* **283**:24546–24553. doi:10.1074/jbc.M800434200

52. Polley S, Huang D-B, Hauenstein AV, Fusco AJ, Zhong X, Vu D, Schröfelbauer B, Kim Y, Hoffmann A, Verma IM, Ghosh G, Huxford T. 2013. A structural basis for IκB kinase 2 activation via oligomerization-dependent trans auto-phosphorylation. *PLoS Biol* **11**:e1001581. doi:10.1371/journal.pbio.1001581

53. Rieke C, Papendieck A, Sokolova O, Naumann M. 2011. Helicobacter pylori-induced tyrosine phosphorylation of IKKβ contributes to NF-κB activation. *Biol Chem* **392**:387–393. doi:10.1515/BC.2011.029

54. Robbins DJ, Zhen E, Owaki H, Vanderbilt CA, Ebert D, Geppert TD, Cobb MH. 1993. Regulation and properties of extracellular signal-regulated protein kinases 1 and 2 in vitro. *J Biol Chem* **268**:5097–106.

55. Rothwarf DM, Zandi E, Natoli G, Karin M. 1998. IKK-gamma is an essential regulatory subunit of the IkappaB kinase complex. *Nature* **395**:297–300. doi:10.1038/26261

56. Sang D, Shu T, Pantoja CF, Ibáñez de Opakua A, Zweckstetter M, Holt LJ. 2022. Condensed-phase signaling can expand kinase specificity and respond to

macromolecular crowding. *Mol Cell* **82**:3693-3711.e10. doi:10.1016/j.molcel.2022.08.016

57. Scheidereit C. 2006. IkappaB kinase complexes: gateways to NF-kappaB activation and transcription. *Oncogene* **25**:6685–705. doi:10.1038/sj.onc.1209934

58. Schrofelbauer B, Hoffmann A. 2011. How do pleiotropic kinase hubs mediate specific signaling by TNFR superfamily members? *Immunol Rev* **244**:29–43. doi:10.1111/j.1600-065X.2011.01060.x

59. Schröfelbauer B, Polley S, Behar M, Ghosh G, Hoffmann A. 2012. NEMO ensures signaling specificity of the pleiotropic IKKβ by directing its kinase activity toward IκBα. *Mol Cell* **47**:111–121. doi:10.1016/j.molcel.2012.04.020

60. Shaul JD, Farina A, Huxford T. 2008. The human IKKbeta subunit kinase domain displays CK2-like phosphorylation specificity. *Biochem Biophys Res Commun* **374**:592–7. doi:10.1016/j.bbrc.2008.07.082

61. Sidrauski C, Walter P. 1997. The transmembrane kinase Ire1p is a site-specific endonuclease that initiates mRNA splicing in the unfolded protein response. *Cell* **90**:1031–1039. doi:10.1016/s0092-8674(00)80369-4

62. Stephenson AA, Taggart DJ, Xu G, Fowler JD, Wu H, Suo Z. 2022. The inhibitor of κB kinase β (IKKβ) phosphorylates IκBα twice in a single binding event through a sequential mechanism. *J Biol Chem* **299**:102796. doi:10.1016/j.jbc.2022.102796

63. Tergaonkar V, Bottero V, Ikawa M, Li Q, Verma IM. 2003. IkappaB kinase-independent IkappaBalpha degradation pathway: functional NF-kappaB activity and implications for cancer therapy. *Mol Cell Biol* **23**:8070–83.

64. Tigno-Aranjuez JT, Asara JM, Abbott DW. 2010. Inhibition of RIP2's tyrosine kinase activity limits NOD2-driven cytokine responses. *Genes Dev* **24**:2666–2677. doi:10.1101/gad.1964410

65. Tu D, Zhu Z, Zhou AY, Yun CH, Lee KE, Toms AV, Li Y, Dunn GP, Chan E, Thai T, Yang S, Ficarro SB, Marto JA, Jeon H, Hahn WC, Barbie DA, Eck MJ. 2013. Structure and ubiquitination-dependent activation of TANK-binding kinase 1. *Cell Rep* **3**:747–58. doi:10.1016/j.celrep.2013.01.033

66. Xu G, Lo Y-C, Li Q, Napolitano G, Wu X, Jiang X, Dreano M, Karin M, Wu H. 2011. Crystal structure of inhibitor of κB kinase β (IKKβ). *Nature* **472**:325–330. doi:10.1038/nature09853

67. Yang J, Garrod SM, Deal MS, Anand GS, Woods VL Jr, Taylor S. 2005. Allosteric network of cAMP-dependent protein kinase revealed by mutation of Tyr204 in the P+1 loop. *J Mol Biol* **346**:191–201. doi:10.1016/j.jmb.2004.11.030

68. Ye Q, Crawley SW, Yang Y, Côté GP, Jia Z. 2010. Crystal structure of the alpha-kinase domain of Dictyostelium myosin heavy chain kinase A. *Sci Signal* **3**:ra17. doi:10.1126/scisignal.2000525

69. Zandi E, Chen Y, Karin M. 1998. Direct phosphorylation of IkappaB by IKKalpha and IKKbeta: discrimination between free and NF-kappaB-bound substrate. *Science* **281**:1360–1363. doi:10.1126/science.281.5381.1360

70. Zandi E, Rothwarf DM, Delhase M, Hayakawa M, Karin M. 1997. The IkappaB kinase complex (IKK) contains two kinase subunits, IKKalpha and IKKbeta, necessary for IkappaB phosphorylation and NF-kappaB activation. *Cell* **91**:243–252. doi:10.1016/s0092-8674(00)80406-7

71. Zhang J, Clark K, Lawrence T, Peggie MW, Cohen P. 2014. An unexpected twist to the activation of IKKbeta: TAK1 primes IKKbeta for activation by autophosphorylation. *Biochem J* **461**:531–7. doi:10.1042/BJ20140444

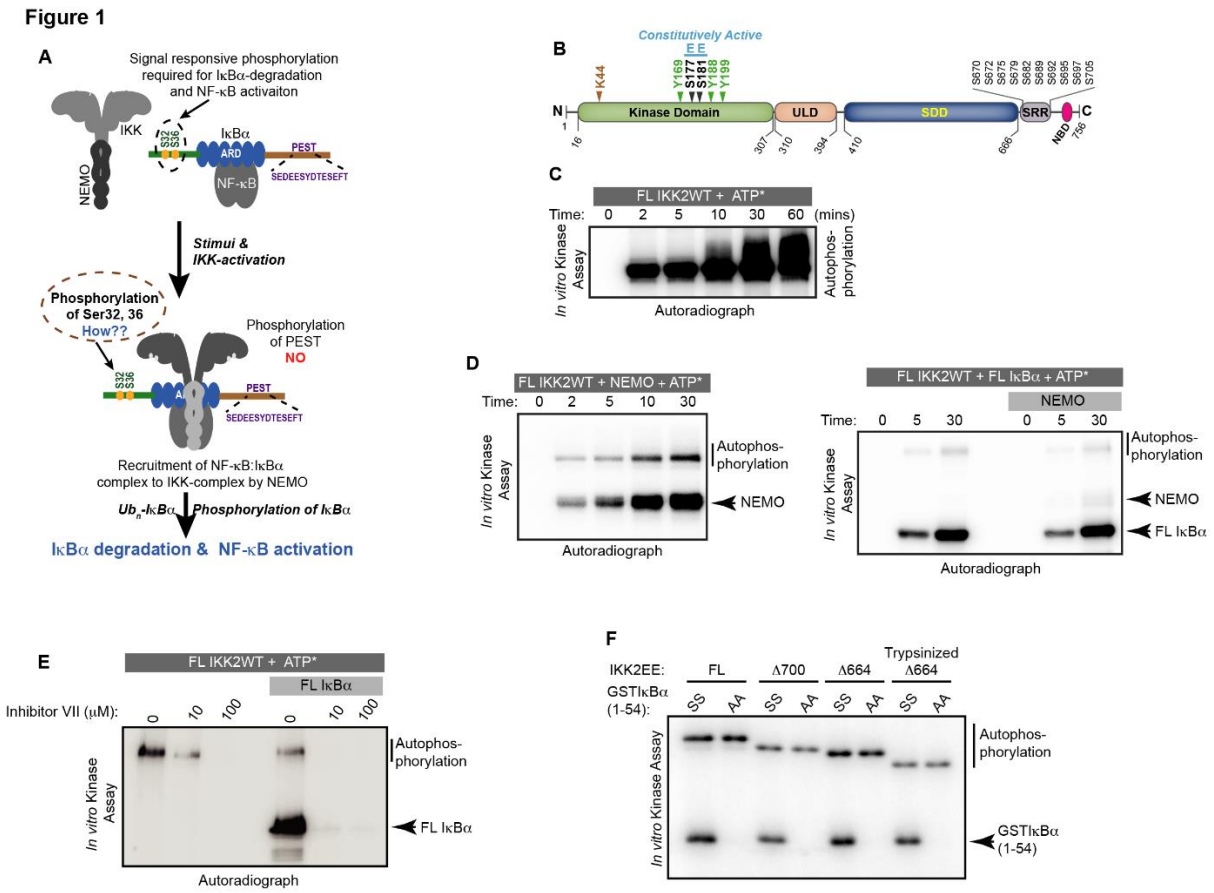

Figure 1: Autophosphorylation of IKK2 at hitherto uncharacterized sites. (A) NEMO is known to remain bound to the IKK-complex pre- and post-stimulation, helps in activation as well as substrate recognition to channelize IKK-activity towards IκBα. However, it is not clear how IKK specifically phosphorylates the Ser32&36 of IκBα. **(B)** Domain organisation of FL IKK2 depicting functional kinase domain (KD), ubiquitin-like domain (ULD), and scaffold dimerization domain (SDD) based on the X-ray structures. Known sites of Ser phosphorylation and NEMO interacting regions at the extreme C-termini are highlighted. Serine and tyrosine residues in the activation loop are shown, mutation of which to Glu renders IKK2 constitutively active. The conserved ATP-interacting Lys (at position 44) is also shown. **(C)** Autophosphorylation of FL IKK2WT upon incubation with radioactive ATP for different time periods in an *in vitro* kinase assay. **(D)** *In vitro* radioactive kinase assays performed to check the effect of NEMO on autophosphorylation of FL IKK2WT (left panel), and that of NEMO and IκBα on autophosphorylation and substrate phosphorylation (right panel) activity of FL IKK2WT. **(E)** Effect of Inhibitor VII on FL IKK2WT autophosphorylation and IκBα substrate phosphorylation at different inhibitor concentrations in a radioactive *in vitro* kinase assay. **(F)** Radioactive kinase assay conducted to check auto- and substrate phosphorylation of full length and deletion constructs of constitutively active form of IKK2 harbouring phosphomimetic Ser177Glu and Ser181Glu mutations.

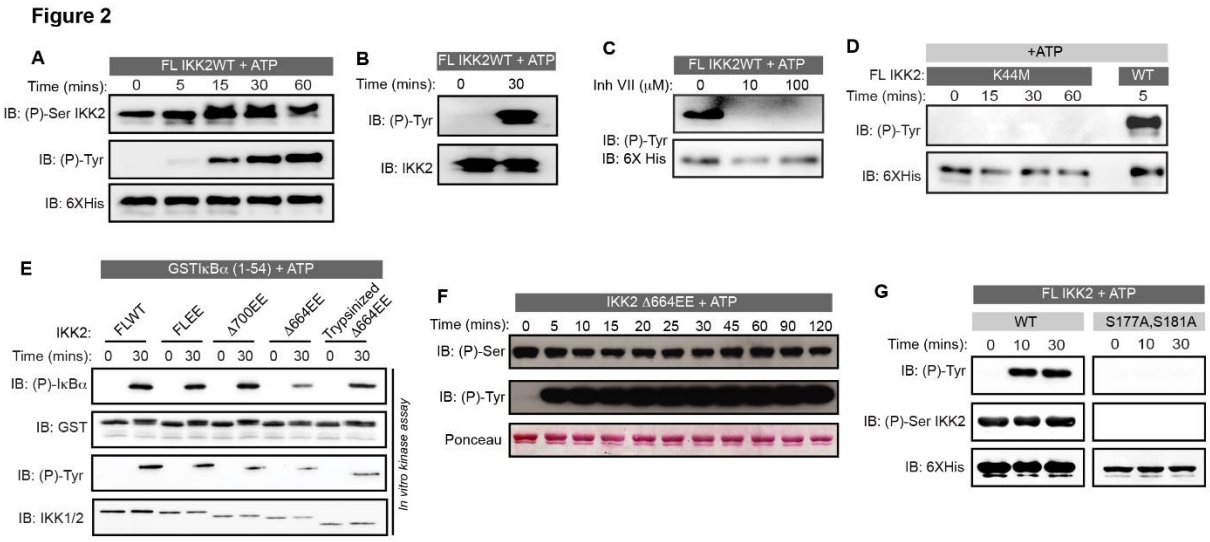

Figure 2: IKK2 possesses autocatalytic dual specificity. (A) *In vitro* kinase assay, followed by immunoblotting with FL IKK2WT using antibodies against phosphor-Ser (177/181) and phospho-Tyr. **(B)** A different commercial source of phospho-Tyr antibody was used to detect the same. **(C)** Effect of Inhibitor VII on tyrosine autophosphorylation of FL IKK2WT. **(D)** Immunoblotting performed with phospho-Tyr antibody to check autophosphorylation of IKK2 mutant K44M at different time points compared to that of IKK2 WT. **(E)** Tyrosine autophosphorylation and substrate phosphorylation of GST (1-54) IκBα in presence of full length and deletion mutants of IKK2 harbouring phosphomimetic Ser177Glu and Ser181Glu mutations. **(F)** *De novo* Auto-phosphorylation of IKK2 on tyrosine monitored by phospho-Ser and phospho-Tyr specific monoclonal antibodies. **(G)** Autophosphorylation and subsequent immunoblot analysis of FLIKK2 mutant S177A, S181A using antibodies against phospho-Ser (177/181) and phospho-Tyr.

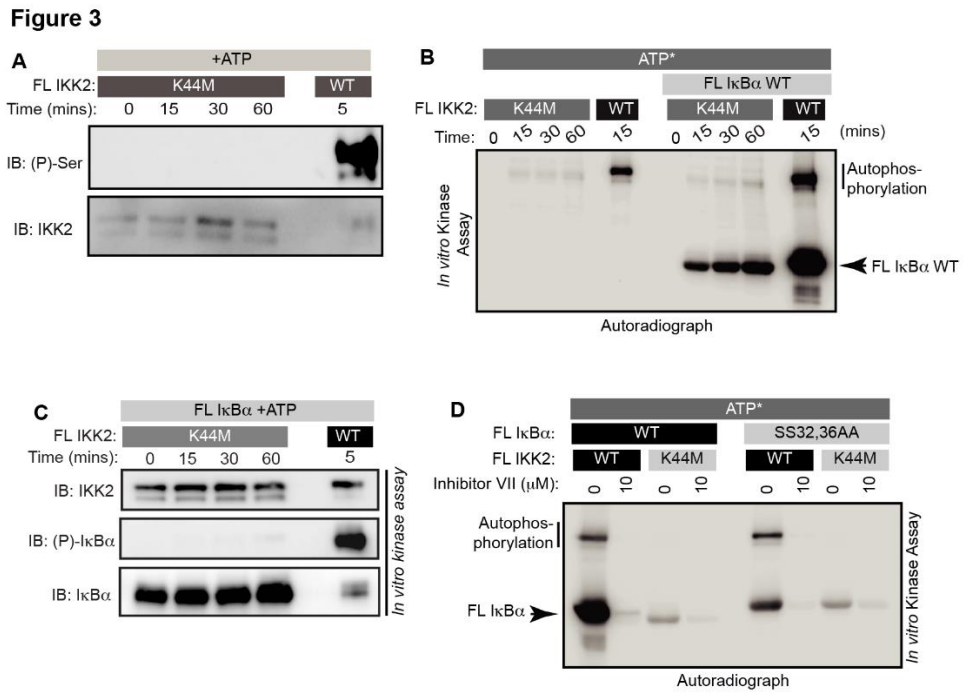

Figure 3: Autophosphorylation of IKK2 is critical to the specificity of IκBα phosphorylation. (A) Immunoblotting performed with phospho-Serine (177/181) antibody to check autophosphorylation of IKK2 mutant K44M at different time points compared to that of IKK2 WT. **(B)** Comparison of substrate and autophosphorylation activities of FL IKK2 WT and K44M mutant in an *in vitro* radioactive kinase assay performed with or without FL IκBα WT as the substrate. **(C)** Residue level specificity of phosphorylation by the FL IKK2 K44M was analysed using an antibody that specifically recognizes phosphor-S32/36 of IκBα. **(D)** Differential sensitivity of specific vs. non-specific phosphorylation by IKK2 as assessed by the effect of Inhibitor VII on FL IKK2 WT and IKK2 K44M using IκBα WT and AA as substrates.

Figure 4

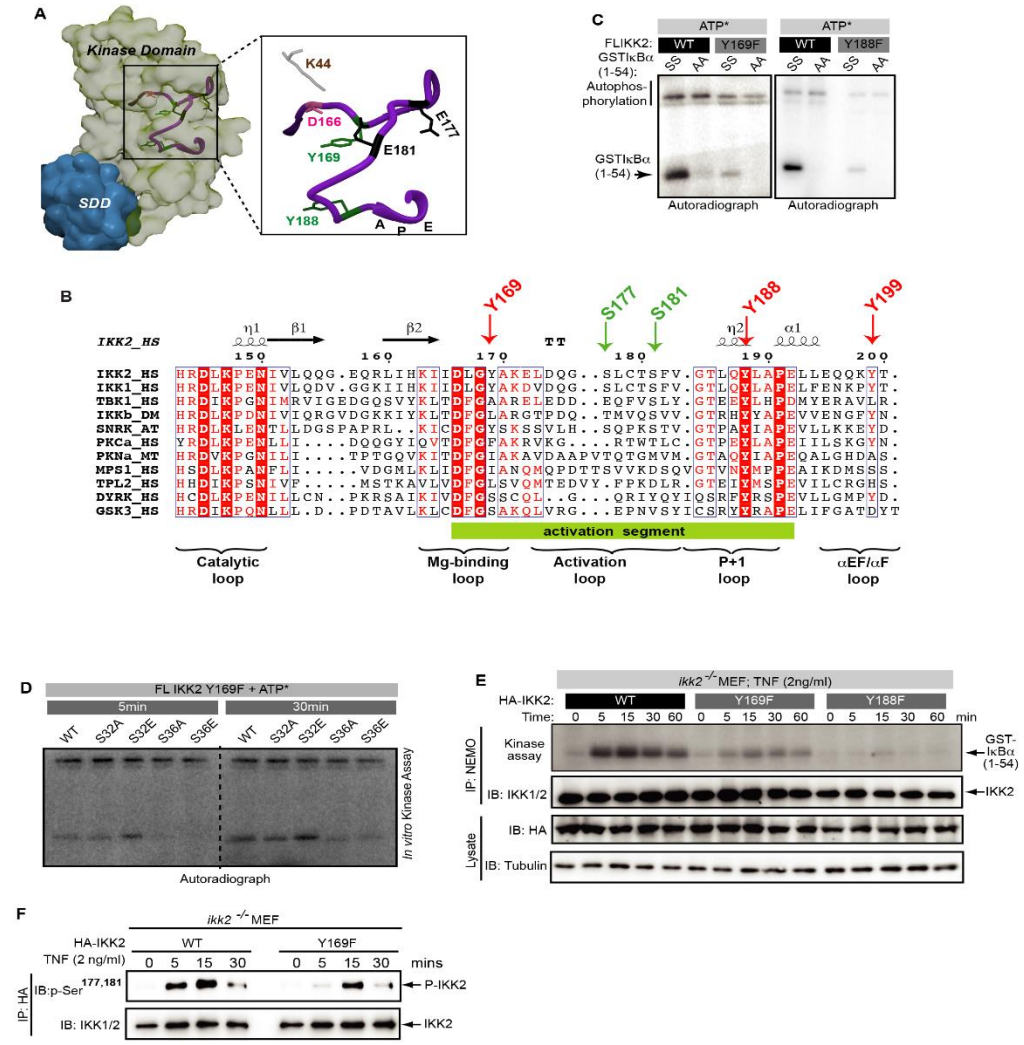

Figure 4: Tyrosine autophosphorylation is critical for IKK2 activity. (A) Position of canonically important residues in the AL (purple ribbon) of IKK2-KD are shown in the context of its structure (PDB ID 4E3C; surface representation; KD is shown light green with respect to the SDD in teal). Autophosphorylated tyrosine residues identified in this study are shown in green. **(B)** Alignment of the activation segment sequences of different IKK family kinases. Conservation of Tyr at the DFG+1 (DLG in case of IKK1 and IKK2) is retained only in a stress response related plant kinase SnRK2, but not in other IKK homologues or any known dual specificity kinases, e.g., DYRK and GSK3β (both contain Ser at that position). Tyr188 (204 in PKA) is conserved. **(C)** Radioactive *in vitro* kinase assay performed with IKK2 Y169F and Y188F mutants using GST (1-54) IκBα WT and AA as substrates. **(D)** Radioactive *in vitro* kinase assay performed with IKK2 Y169F mutant with a range of GST (1-54) IκBα mutants where the substrate phosphorylation signal is abolished in case of S36 A/E IκBα. **(E)** Severe reduction in TNFα-induced IKK activity in *ikk2-/-* MEF-3T3 cells reconstituted with mutant (Y169F and Y188F) IKK2s compared to wild-type. Kinase assay was performed with IKK immunoprecipitated (IP-ed) with anti-NEMO antibody from whole cell extract. **(F)** AL-serine phosphorylation status of IKK2 WT and Y169F was assessed in reconstituted MEFs post-stimulation with TNF-α after immunoprecipitating the kinase with monoclonal anti-HA antibody.

Figure 5

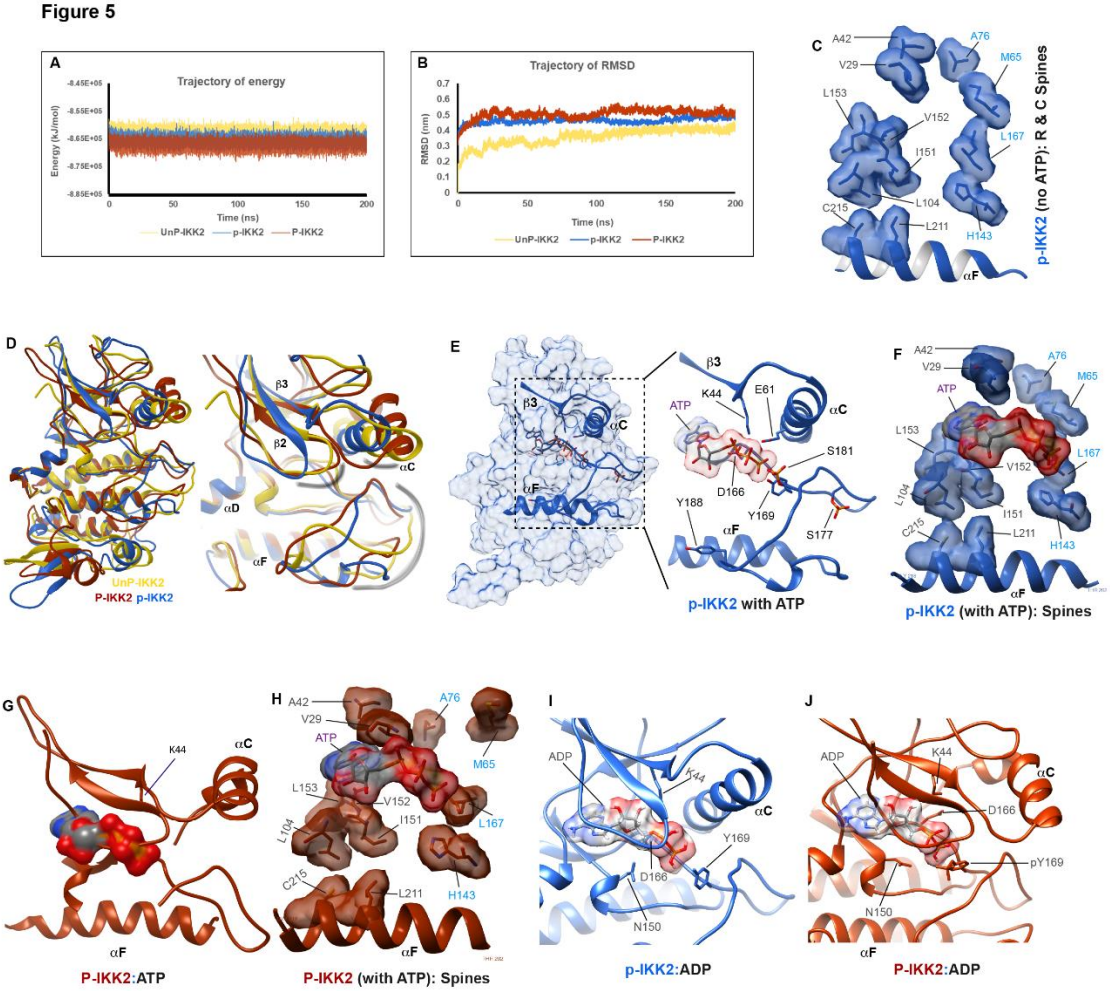

Figure 5: Structural analyses of IKK2 autophosphorylation. (A) Molecular dynamics (MD) simulations of all three differently phosphorylated states of IKK2 was performed. 200ns trajectory of energy for each state is shown in golden yellow, blue and copper red representing UnP-IKK2, p-IKK2 and P-IKK2, respectively. Same color coding has been followed throughout this figure and the corresponding supplementary figure. **(B)** 200ns trajectory of RMSD for each state is shown**. (C)** Residues forming canonical R- (labelled in blue) & C-spines (labelled in dark gray) representative of an active conformation in p-IKK2 are shown. **(D)** Superposition of structures representing the differently phosphorylated states post 200ns MD simulation. Relevant sections, e.g., activation loop, αC-helix, Gly-rich loop areas are highlighted in the right panel. **(E)** ATP-bound p-IKK2 structure is depicted. In the right panel, relevant residues are highlighted. Y169 is found in a position poised for autophosphorylation. **(F)** ATP completes the desired continuum of R- & C-spine observed in active kinase conformations. **(G)** P-IKK2 cannot accommodate ATP in its cleft, and αC-helix is displaced. **(H)** M is moved away from the R-spine, failing to form canonically active conformation of R- & C-spines. **(I & J)** ADP-bound p-IKK2 and P-IKK2 states are shown, respectively. Both p-IKK2 and P-IKK2 states can accommodate ADP in their respective clefts.

Figure 6

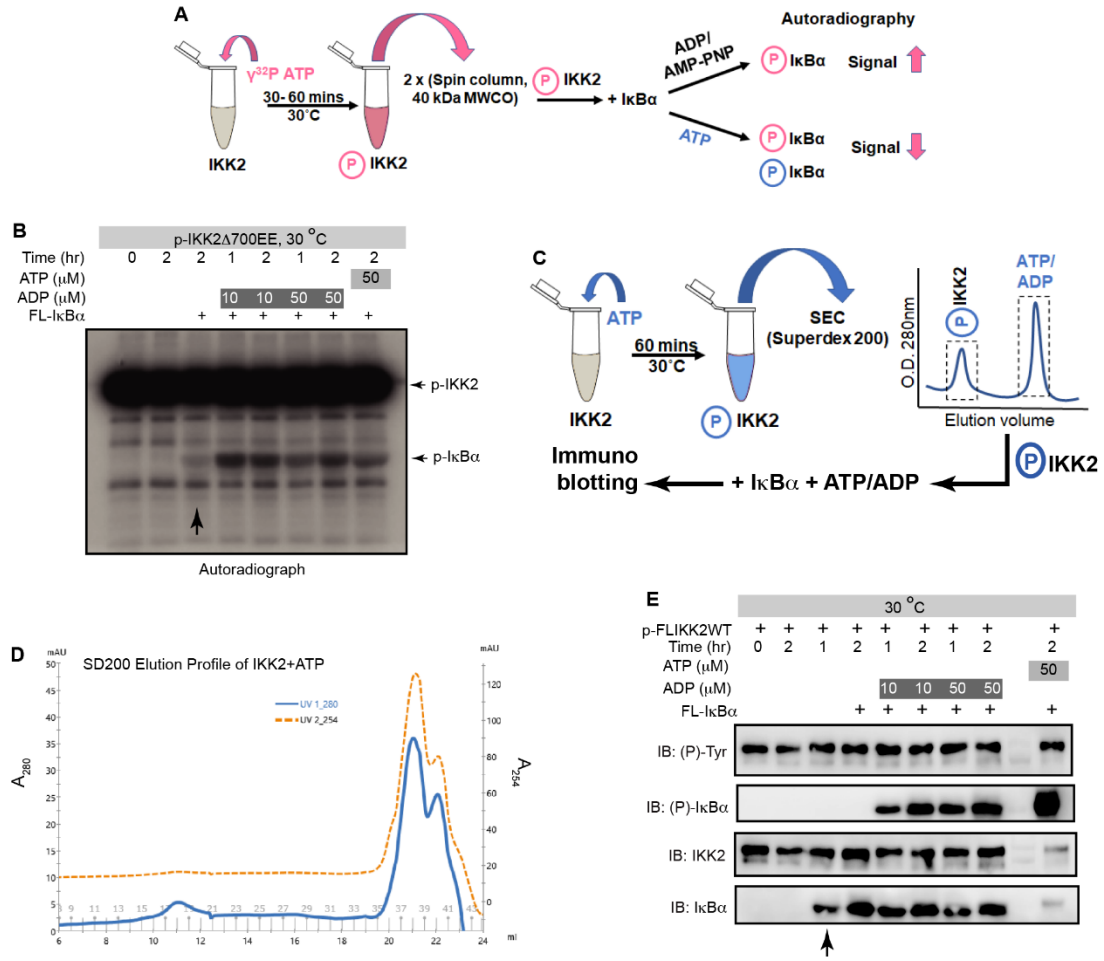

Figure 6: Freshly autophosphorylated IKK2 relays phosphates to IκBα. (A) A schematic representation of the experiment performed to monitor the path traversed by phosphate(s) from p-IKK2 to substrate by autoradiography detection method. **(B)** Purified autophosphorylated (radiolabelled) IKK2 transfers its phosphate to IκBα substrate in absence of any nucleotide, and transfer efficiency is enhanced upon addition of ADP or ATP. **(C)** A schematic representation of the experiment performed to monitor the path traversed by phosphate(s) from p-IKK2 to substrate by immunoblotting detection method. **(D)** Elution profile of the size exclusion chromatography run of p-IKK2 to get rid of excess unlabelled ATP performed in Superdex200 10/30 increase. **(E)** Purified autophosphorylated (cold) IKK2 transfers its phosphate to IκBα substrate with enhanced transfer efficiency upon addition of ADP or ATP.

Figure 7

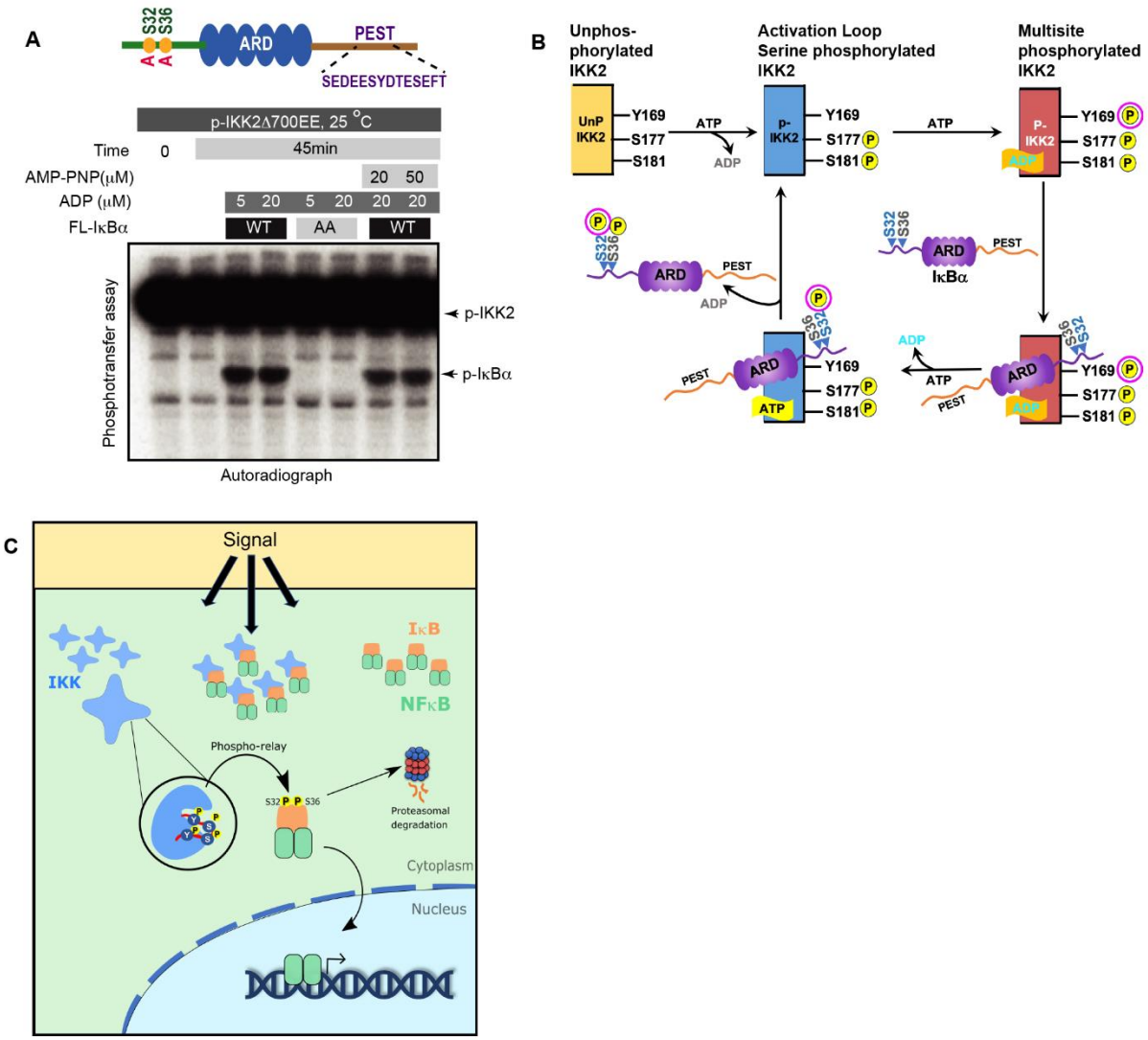

Figure 7: Specificity and fidelity of phosphotransfer by IKK2 to IκBα. (**A**) AMP-PNP can support efficient phosphotransfer. Also, phosphotransfer is observed in IκBα WT but not in S32,36Ala double mutant. Domain organization and position of relevant S/T/Y residues of IκBα are shown above the autoradiograph. **(B)** A detailed scheme of reactions showing IKK2-activation and subsequent phosphorylation of the signal-responsive S32,36 on IκBα through a phosphoenzyme intermediate. **(C)** A cartoon representation of the proposed model of NF-κB activation by IKK2 employing direct phosphotransfer to IκBα.

Figure S1

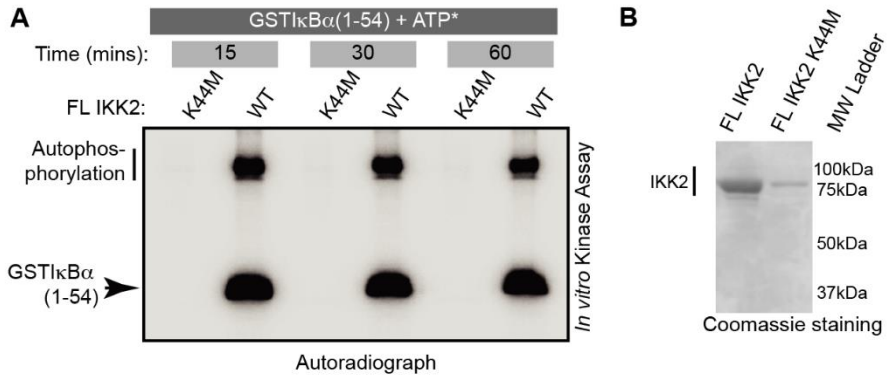

Figure S1: (A) Autoradiograph of *in vitro* kinase assay reactions carried out with FL IKK2 WT and K44M using GST (1-54) IκBα as the substrate as a function of time. **(B)** Coomassie stained SDS-PAGE showing purity of some of the IKK2 proteins used in this study.

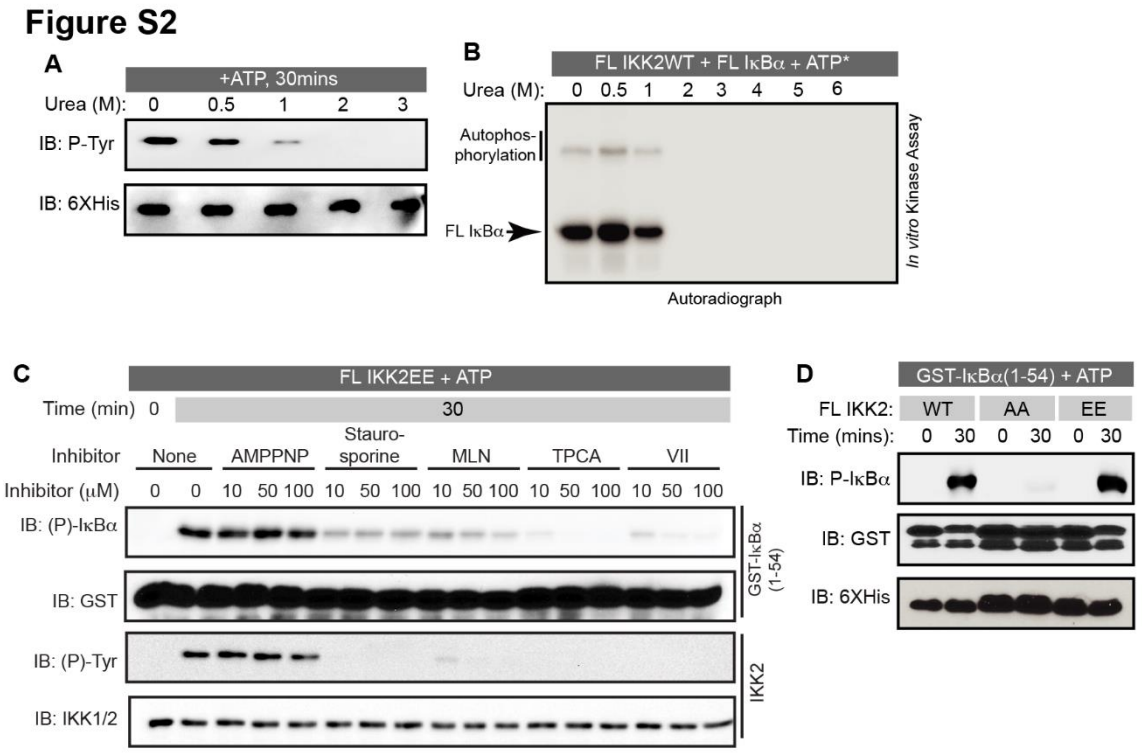

Figure S2: (A) Effect of increasing concentration of urea on tyrosine autophosphorylation of FL IKK2WT assessed in an *in vitro* kinase assay. **(B)** Radioactive *in vitro* kinase assay performed with increasing concentration of urea up to 6M to check auto- and substrate phosphorylation. **(C)** Inhibition of both substrate phosphorylation and tyrosine autophosphorylation activities of IKK2 checked in presence of common kinase inhibitors such as AMPPNP and Staurosporine, highly specific IKK2 inhibitors TPCA, Calbiochem Inhibitor VII and MLN120B. **(D)** Mutation of AL-serines to non-phosphorylatable alanine (FL IKK2 S177A,181A double mutant) debilitates its kinase activity towards S32,36 of IκBα compared to WT or EE version of IKK2 as observed in an *in vitro* kinase assay.

Figure S3

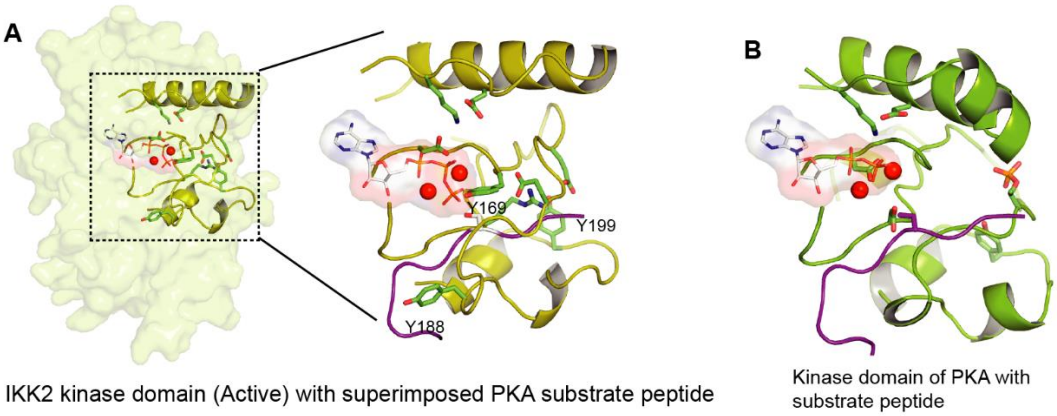

Figure S3: (A) A close-up view of the active site in active form in the context of the entire kinase domain of IKK2. Three tyrosines (Y169, Y188 and Y199) in immediate vicinity of active sites are highlighted. Position of ATP is modelled based on the structure of PKA. **(B)** Substrate bound PKA in its active form; phosphorylatable serine of the substrate peptide (in magenta) is highlighted.

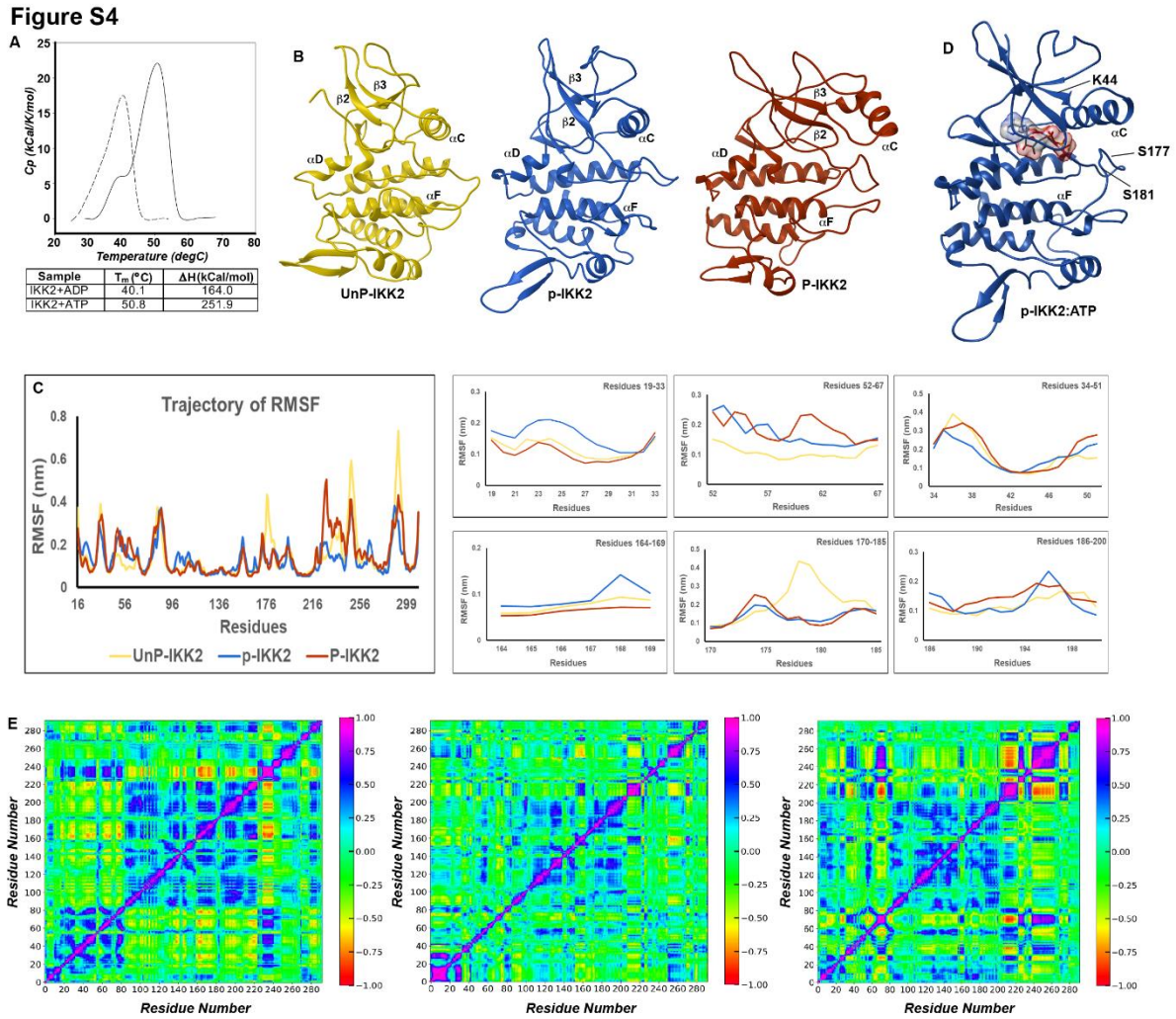

Figure S4: (A) A differential scanning calorimetry (DSC) thermogram showing a striking enhancement in folding stability of IKK2 upon ATP-treatment. **(B)** Ribbon representation of different phosphorylated versions of IKK2 are shown: UnP-IKK2 in golden yellow, p-IKK2 in blue and P-IKK2 in copper red. **(C)** Trajectories of RMSF for these structures are shown (left panel). For clarity, different regions of the KD are shown in the right. **(D)** ATP-bound structure of p-IKK2 is shown. **(E)** Dynamic cross-correlation matrix (DCCM) or contact map of each structure reveals phosphorylation-induced local as well as allosteric changes.

Figure S5

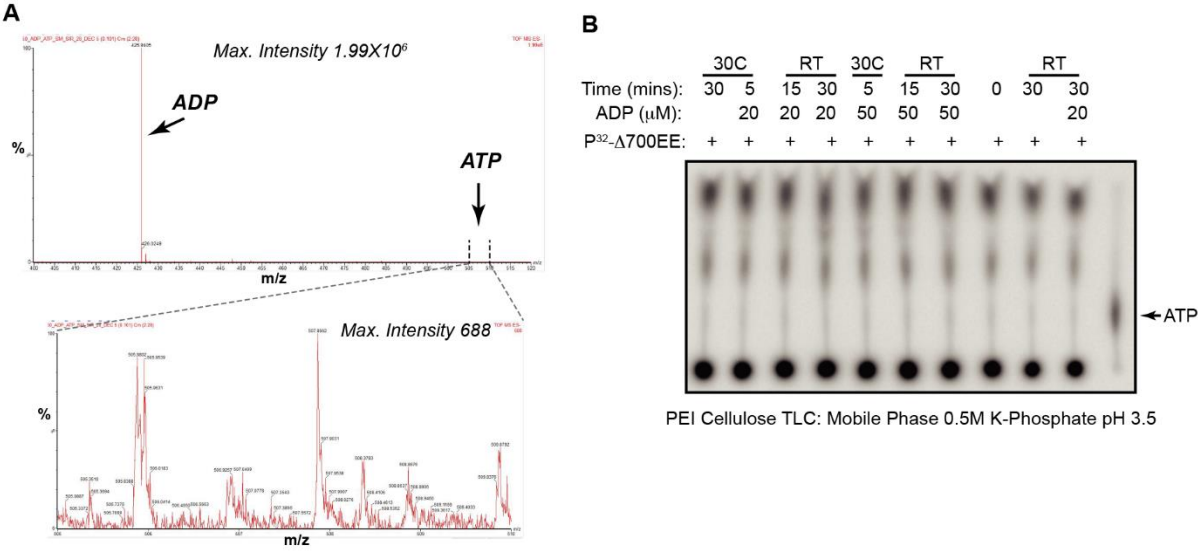

Figure S5: (A) ESI-MS scan of the ADP used in this assay system showing negligible trace, if any, of ATP at 50μM ADP concentration. **(B)** Regeneration of ATP, if any, through microscopic reversibility was checked by TLC in a variety of conditions. γ-P^{32} was used as the control/standard.

Materials and methods:

Reagents and Cell culture:

Monoclonal mouse anti-IκBα (L35A5) (catalogue number: 4814), mouse anti-Phospho-IκBα ($Ser^{32/36}$) (5A5) (catalogue number:9246) and rabbit anti-Phospho-IKKα/β ($Ser^{176/180}$) (16A6) (catalogue number: 2697) were from Cell Signaling Technology (CST). Monoclonal mouse anti-IKKβ (10AG2) (catalogue number: NB100-56509) was from Novus Biologicals. Polyclonal rabbit anti-6XHis (catalogue number: BB-AB0010) was from BioBharti Life Science. Monoclonal mouse anti-Phospho-Tyrosine (catalogue number: 610000) was from BD Biosciences. Polyclonal rabbit anti-GST (catalogue number: 924801), monoclonal mouse anti-HA 11 epitope (catalogue number: 901502) and mouse anti-Tubulinβ3 (catalogue number: 657402) were from BioLegend. Polyclonal rabbit anti-IKKα/β (H-470): sc7607 was from Santa Cruz Biotechnology (has been discontinued) and mouse anti-Phospho-Serine Q5 (catalogue number: 37430) was from Qiagen. Horseradish peroxidase-conjugated secondary antibodies against rabbit (catalogue number: 31460) and mouse IgG (catalogue number: 31430) were Pierce antibodies from Thermo Scientific. Adenosine-5'-Triphosphate (ATP), Disodium trihydrate (catalogue number: A-081-25) was from Gold Biotechnology and Adenosine Diphosphate (ADP) (Reference number: V916A) provided in ADP-Glo™ Kinase assay (catalogue number: V6930) from Promega. Recombinant murine TNF-α used was from Roche.

Sf9 cells used for expressing proteins with baculovirus system was procured from Gibco™ Sf9 cells in Sf-900™ III SFM, Thermo Scientific (catalogue number: 12659017) and maintained in Gibco™Sf-900™ III SFM, Thermo Scientific (catalogue number: 12658019).

Protein expression and purification:

IKK2 (WT and other constructs):

Wild-type and mutant IKK2s were purified following a published protocol (Polley et al, 2013). Sf9 cells (Gibco™ Sf9 cells in Sf-900™ III SFM) at a density of 1.5-2 millions/ml were infected with high titre viral stock (generally after P3 stage) at a ratio of 1:100 or 1:50 as

optimized for higher expression level as judged by a pilot experiment performed previously, and grown for 48 hours upon infection. Cells were harvested and lysed by sonication in a buffer containing 25 mM Tris-HCl pH 8.0, 200 mM NaCl, 10% Glycerol, 5 mM β-Mercaptoethanol (β-ME), 10 mM Imidazole, 20 mM β-glycerophosphate, 10 mM NaF, and 1 mM sodium orthovanadate and 1X Protease Inhibitor Cocktail (PIC, Sigma). The lysate was clarified by centrifugation at 20,000 x g for 45 minutes at 4˚C and incubated with Ni-NTA agarose resin (Qiagen, catalogue number: 30230) pre-equilibrated with lysis buffer for 2 hours at 4˚C. The resin was subsequently washed with lysis buffer containing 30mM Imidazole. Protein was eluted with lysis buffer containing 250mM Imidazole. Protein fractions were analysed on SDS-PAGE, pooled together and either flash frozen or subjected to size-exclusion chromatography on Superdex 200 Increase 10/300 GL (Cytiva) column equilibrated with 20mM Tris-HCl pH 8.0, 200mM NaCl, 10% Glycerol and 2 mM DTT. To make untagged IKK2, protein fractions eluted from the Ni-NTA resin of desired purity was treated with TEV-protease at a ratio of 50:1 (weight by weight, IKK2: TEV) in the cold room for more than 10 hours after addition of 1 mM of EDTA, the resulting protein mix was then loaded on to the SEC as described above. To prepare autophosphorylated IKK2, the fractions with desired purity level were treated with 0.5-1 mM of ATP,10 mM of $MgCl_2$ and phosphatase inhibitors and the autophosphorylation reaction was carried out at 27˚C for 1 hour. Resulting protein solution was then concentrated in a YM30-concentrator and loaded onto Superdex 200 Increase 10/300 GL column. Elution fractions from the size-exclusion step were analysed on SDS-PAGE and peak fractions of desired quality (Cytiva) were pooled together and concentrated using a YM30 Centriprep or Centricon devices (Millipore) depending upon the volume of the sample and flash frozen immediately.

IκBα (WT, mutant and other constructs):

His-tagged full length and GST-tagged deletion (1-54) constructs of IκBα (both the wild-type and Ser32Ala, Ser36Ala, Ser32,36Ala single and double-mutant versions) were expressed in *E. coli* Rosetta2 (DE3). The cells were grown overnight at 16˚C after 0.3 mM IPTG induction. The cell pellet was resuspended in 40 ml of Lysis Buffer (25 mM Tris pH 7.5,

200 mM NaCl, 10 mM imidazole, 10% Glycerol, 5 mM β-mercaptoethanol, and 1 mM PMSF). The cells were lysed by using sonicator keeping the cell suspension chilled on ice. The lysate was clarified by centrifugation at 15,000 x g for one hour at 4°C. About 3 ml of Ni-NTA Agarose resin was equilibrated with lysis buffer, and the clarified lysate (supernatant) was mixed with it later. The protein was allowed to bind the resin by incubating for 2 hours on a rotary mixer in a 4°C room. The resin was washed with the lysis buffer containing 500 mM NaCl (high salt wash) for about 50 CV to clear out non-specific proteins from binding. Then the resin was thoroughly washed with the lysis buffer containing 20 mM imidazole. His-tagged IκBα protein was eluted under gravity flow, using elution buffer (the lysis buffer containing 250 mM imidazole). ~1 ml volume of each fraction was collected. [For GST tagged proteins, Glutathione Sepharose resin (Cytiva, catalogue number: 17-5279-01] was used and elution was performed with the help of reduced glutathione). The main elution fractions were subjected to size-exclusion chromatography (SEC) on a HiLoad 16/600 pg Superdex 200 column (Cytiva) and the gel run revealed cleaner protein fractions. The peak fractions were saved and stored at -80˚C.

NEMO (WT, mutant and other constructs):

NEMO FL, NEMO double mutant C76A C95S (site directed mutagenesis done in pET24d vector) and NEMO (44-196) (truncates in pET24d) were expressed in *E. coli* Rosetta2 DE3 cells. The cells were grown overnight at ~21˚C after 0.25 mM IPTG induction (at 0.3-0.4 O.D.) and 50-100 μM Zn^{2+}. [OR The cells were grown overnight (~17 hours) at 16˚C after 0.1 mM IPTG induction (at 0.2-0.3 O.D.) and 50-100 μM Zn^{2+}]. The cell pellet was resuspended in 40 ml of Lysis Buffer (25 mM Tris pH 7.5, 200 mM NaCl, 10 mM imidazole, 10% Glycerol, 5 mM β-mercaptoethanol, 20μM $ZnCl_2$, 0.5 M urea (acting like an osmolyte). Rest of the steps performed were typical to a Ni-NTA purification as described above. The main elution fractions were subjected to size-exclusion chromatography on a HiLoad 16/600 pg Superdex 200 column (Cytiva) and the cleaner peak fractions were stored at -80˚C.

Kinase Assay with purified proteins:

Typically, 50-100 ng (unless mentioned otherwise) of purified kinase was used in each *in vitro* kinase reaction. 0.5-1μg of IκBα substrate (full-length or GST-tagged 1-54) was incubated with kinase for 30 mins or indicated time periods at 27˚C in presence of 20μM ATP with 0.1μCi of γ-P32-ATP in case of radioactive assay or 50-100 μM ATP in case of Western blot assay in a reaction buffer containing 20mM HEPES pH 7.5, 100mM NaCl, 15mM $MgCl_2$, 2mM DTT, 0.2mM Na_3VO_4, 10mM NaF, 20mM β-Glycerophosphate. Reaction was stopped by heating the samples at 95˚C for 5 mins after the addition of 1X-Laemmli buffer. Samples were run on 8 or 10% SDS-PAGE. For radioactive assays, the gel was then dried and analysed either by film or phosphor-imaging. For Western blot assays, proteins from gel were electro-transferred onto nitrocellulose/PVDF membrane and probed with desired antibodies. Phosphorylated tyrosine and serine residues were detected using monoclonal antibodies against phospho-tyrosine and phospho-serine.

IP-Kinase assay:

Immortalized *ikk2*$^{-/-}$ mouse embryonic fibroblast 3T3 cells were reconstituted by retroviral transduction with HA-tagged WT or mutant pBABE-IKK2 constructs. Stable expression of IKK2 was first confirmed by immunoblotting. Cells were then stimulated with recombinant murine TNF-α (Roche) at 70-80% cell confluency. IKK complex was immunoprecipitated from whole cell extracts using a NEMO-specific antibody (BD) and Protein A agarose (Upstate) for 2 hrs in the cold room. Whole cell extract used was pre-cleared by incubation with Protein A agarose bead for an hour. Immunoprecipitated complex was washed extensively, including a final washing step with the kinase assay buffer devoid of ATP and incubated with GST-IκBα (1-54) and 20 μM ATP and 5 μCi of γ-^{32}P-ATP for 30 mins at 30˚C in kinase assays. Reactions were stopped by addition of 2X-Laemmli SDS buffer to samples and heating at 95˚C for 5 mins. Reaction products were resolved on a 12% SDS PAGE. Extent of substrate phosphorylation was measured by cutting out the appropriate area of the gel containing the substrate and subjecting it to phosphor-imaging (Typhoon, Cytiva) after drying. As a control, amount of IKK2 in each reaction was estimated by transferring IKK2 containing gel area onto nitrocellulose membrane and probing it with anti-IKK1/2 antibody.

Sample preparation for LC-MS/MS analyses for Tyrosine phosphorylation detection:

Protein samples were diluted in TNE (50mM Tris pH 8.0, 100mM NaCl, 1mM EDTA) buffer. RapiGest SF reagent (Waters Corp.) was added to the mix to a final concentration of 0.1% and samples were boiled for 5 min. Tris (2-carboxyethyl) phosphine (TCEP) was added to a final concentration of 1mM and the samples were incubated at 37˚C for 30 min. Subsequently, the samples were carboxymethylated with 0.5 mg/ml of iodoacetamide for 30 min at 37˚C followed by neutralization with 2mM final concentration of TCEP. Proteins samples prepared as above were digested with trypsin and GluC protease (Promega) at a protease: protein ratio of - 1:50 for overnight at 37˚C. RapiGest was degraded and removed by treating the samples with 250 mM HCl at 37˚C for 1 h followed by centrifugation at 14000 rpm for 30 min at 4˚C. The soluble fraction was then added to a new tube and the peptides were extracted and desalted using C18 desalting columns (Thermo Scientific).

LC-MS/MS analysis:

Trypsin-digested peptides were analysed by ultra-high-pressure liquid chromatography (UPLC) coupled with tandem mass spectroscopy (LC-MS/MS) using nano-spray ionization. The nano-spray ionization experiments were performed using a TripleTOF 5600 hybrid mass spectrometer (ABSCIEX) interfaced with nano-scale reversed-phase UPLC (Waters corporation nano ACQUITY) using a 20 cm-75-micron ID glass capillary packed with 2.5 µm C18 (130) CSHTM beads (Waters corporation). Peptides were eluted from the C18 column into the mass spectrometer using a linear gradient (5–80%) of Acetonitrile (ACN) at a flow rate of 250 µl/min for 1h. The buffers used to create the ACN gradient were: Buffer A (98% H2O, 2% ACN, 0.1% formic acid, and 0.005% TFA) and Buffer B (100% ACN, 0.1% formic acid, and 0.005% TFA). MS/MS data were acquired in a data-dependent manner in which the MS1 data was acquired for 250ms at m/z of 400 to 1250 Da and the MS/MS data was acquired from m/z of 50 to 2,000Da. The Independent data acquisition (IDA) parameters were as follows; MS1-TOF acquisition time of 250 milliseconds, followed by 50 MS2 events of

48 milliseconds acquisition time for each event. The threshold to trigger MS2 event was set to 150 counts when the ion had the charge state +2, +3 and +4. The ion exclusion time was set to 4 seconds. Finally, the collected data were analysed using Protein Pilot 4.5 (ABSCIEX) for peptide identifications.

ESI-MS analyses of ADP:

50 μM of ADP solution was prepared to be analysed by Electrospray Ionisation Mass Spectrometry (ESI-MS). It was performed in a Xevo G2-XS QToF mass spectrometer (Waters Corporation) using capillary at 3kV, with voltage parameters of sampling cone at 40V and source offset at 80V. The source temperature was set at 100˚C and desolvation temperature at 40˚C. The gas flow rates were as follows: Cone gas flow rate at 50 litre/hr and desolvation gas flow rate at 400 litre/hr. The sample was passed at 5 μl/min flow rate. The MS data was acquired for a mass range of 50-2000 m/z and the acquisition time was 1 minute.

Radioactive Phosphotransfer assay:

Phosphotransfer assays were performed in a wide range of concentration of IKK2, IκBα and ATP. Typically, 10 μM purified IKK2 protein was first autophosphorylated in presence of 100-200 nM of γ32P-ATP (PerkinElmer) in kinase assay buffer for 1 hour at 30˚C. 70 μl of the resulting reaction mixture was first passed through a Micro Bio-Spin Bio-Gel P-30 spin column (Bio-Rad; 40 kDa MWCO) equilibrated with 20 mM HEPES pH 7.9, 100 mM NaCl, 0.2 mM Na_3VO_4, 10 mM NaF, 20 mM β-Glycerophosphate, 2 mM DTT, 2 mM EDTA and 1X protease inhibitor cocktail. Eluted protein was subjected to another round of buffer exchange on a Bio-Gel P-30 column equilibrated with the same buffer mentioned above devoid of EDTA and containing 15 mM $MgCl_2$. Phosphorylated IKK2 thus obtained was used in phosphotransfer reaction. 2-3 μM of Phosphorylated IKK2 was incubated with 10-20 μM of WT or mutant IκBα protein at 30˚C in kinase assay buffer in a total volume of 20 μl for different time periods as indicated in Figure 5B and 6A. The reactions were stopped by addition of 10 μl of 4X Laemmli SDS-buffer containing 100 mM EDTA to samples and heating at 95˚C for 5 mins. Different concentration of ADP or ATP was added to the assay to assess the role of

these nucleotides in phosphotransfer efficiency. Routinely, 10-15µl of reaction products were resolved on 10% SDS PAGE and radiolabelled samples were monitored by phosphor imaging of the dried gel on a Typhoon scanner. For the phosphotransfer reaction described in Figure 4a, 10 µM purified IKK2 was autophosphorylated with of 100 nM of γ^{32}P-ATP in presence of 40 µM of cold ATP.

Phospho-transfer assay with cold ATP:

About 10 µM of purified FL IKK2WT was treated with 100 µM of cold ATP in kinase assay buffer (containing 1X protease inhibitor cocktail) for one hour at 30˚C. The resulting reaction mixture was then loaded onto a Superdex 200 increase 10/300 GL (24ml bed volume, Cytiva) SEC column to purify autophosphorylated FL IKK2WT separated from excess ATP. SEC was performed in buffer containing 20 mM HEPES, 100 mM NaCl, 20 mM β-glycerophosphate, 10 mM NaF, 0.2 mM Na_3VO_4 and 2 mM DTT. The elution fractions containing phosphorylated IKK2 were incubated with FL IκBαWT in presence of different concentrations of ATP or ADP at different time points (as mentioned in Figure 3f) at 30˚C. The reactions were stopped by adding 4X Laemmli SDS dye, heated at 95˚C for 5 minutes and were run on a 10% SDS-PAGE. This was followed by immunoblotting and detection was done using monoclonal antibodies against phospho-tyrosine and phospho $Ser^{32/36}$ IκBα.

Molecular Dynamics Simulation

The kinase domain structure of IKK2 (PDB ID: 4E3C), spanning residues 16 to 310, was obtained from the PDB database. We created unphosphorylated forms (at Ser177 & Ser181) and two phosphorylated forms (phosphorylated at Ser177 & Ser181 and at Tyr169 & Ser177 & Ser181) of IKK2 using UCSF CHIMERA software. These structures underwent molecular dynamics (MD) simulations using the GROMACSv2023.1 simulation package, enabling a comparative analysis of their structural and energetic stability. The Charmm36 force field was applied to generate coordinates and topology files for the IKK2 structures. For simulation, a cubic box was defined and filled with TIP3 water molecules. Sodium and chloride ions were added to neutralize the three systems. The system underwent two-stage

minimization using steepest-descent and conjugate-gradient algorithms. Equilibration was carried out under NVT (constant particle number, volume, and temperature) and NPT (constant particle number, pressure, and temperature) conditions for 200 ps at 300 K and 1 atm pressure. MD simulations were conducted for 200 ns for each protein. To assess global structural changes, Root Mean Square Deviation (RMSD) analysis was employed, while Root Mean Square Fluctuation (RMSF) analysis revealed the overall and local motion/flexibility of the proteins. The *gmx_energy* module was utilized to compute energy during simulation, and *gmx_sasa* was employed to determine the solvent accessible surface area (SASA) of the protein. To understand the correlations of the atomic motions in different regions, the dynamic cross-correlation analysis was carried out. The initial step of dynamic cross-correlation analysis was to construct the covariance matrix which examines the linear relationship of atomic fluctuations for individual atomic pairs. The covariance matrix was calculated using the *gmx_covar* tool. Dynamic cross-correlation matrices (DCCM) were calculated from the C_α-trace covariance matrix principal components. Results are displayed as a color coded with a value of −1 indicated completely anti-correlated motions and a value of +1 indicating completely correlated motions.

Molecular Docking Analysis

The terminal structures from the simulations (200th ns) doubly phosphorylated IKK2 at S177,S181 (p-IKK2) form was subjected to molecular docking analysis using ATP and ADP as ligands, allowing for comparison of binding affinities. LeDock software was employed for ligand-protein docking. The top 100 docking solutions were extracted. The p-IKK2:ATP poses were compared with available kinase:ATP complexes, e.g., PKA:ATP complex (PDB ID 1ATP). The pose that resembled most with the pose found in PDB ID 1ATP was chosen for further analysis. p-IKK2:ADP poses were also compared likewise, where IRE1:ADP (PDB ID 2RIO) complex was chosen for comparison and the pose closest to that in PDB ID 2RIO was chosen for further analysis.

For assessing the ability of P-IKK2 to accommodate ATP or ADP, the MD-simulation derived P-IKK2 structure was superimposed on the p-IKK2 structure bound to ATP/ADP, and compared as described.